JCI The Journal of Clinical Investigation

Systemic silencing of PHD2 causes reversible immune regulatory dysfunction

Atsushi Yamamoto, … , Peter J. Ratcliffe, Chris W. Pugh

J Clin Invest. 2019. https://doi.org/10.1172/JCI124099.

Research In-Press Preview Immunology Therapeutics

Graphical abstract

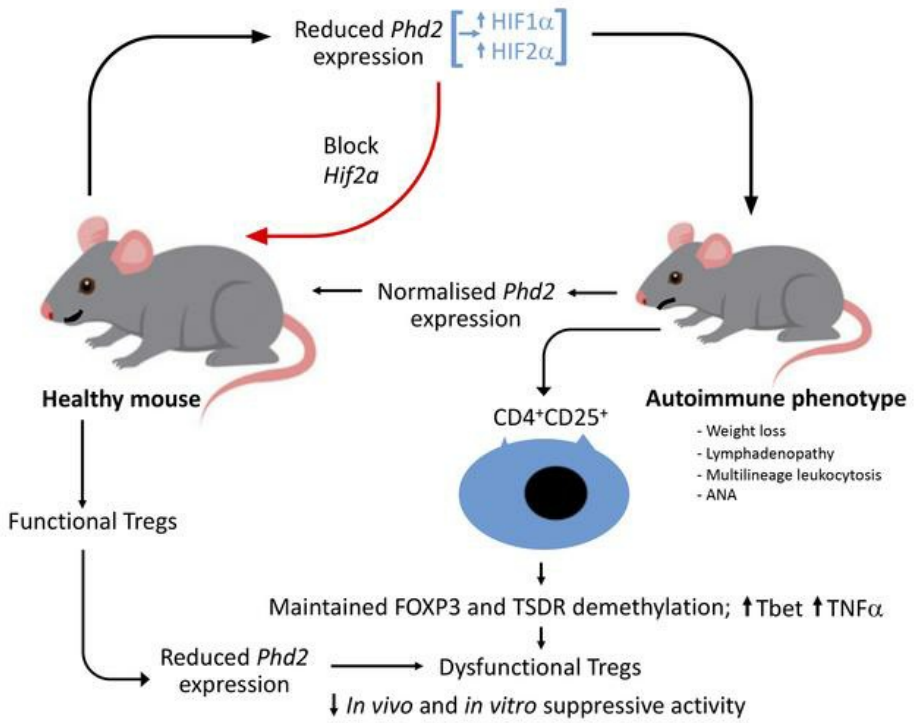

SYSTEMIC SILENCING OF PHD2 CAUSES REVERSIBLE IMMUNE REGULATORY DYSFUNCTION

Atsushi Yamamoto* 1

Joanna Hester* 2

Philip S Macklin 1

Kento Kawai 2

Masateru Uchiyama 2

Daniel Biggs 3

Tammie Bishop 1

Katherine Bull 4

Xiaotong Cheng 1

Eleanor Cawthorne 4

Mathew L. Coleman 4, 5

Tanya L Crockford 4

Ben Davies 3

Lukas E Dow 6

Rob Goldin 7

Kamil Kranc 8

Hiromi Kudo 7

Hannah Lawson 8

James McAuliffe 9

Kate Milward 2

Cheryl L Scudamore 10

Elizabeth Soilleux 11

Fadi Issa** 2

Peter J Ratcliffe** 1, 9, 12

Chris W Pugh** *** 1

Nuffield Department of Medicine, University of Oxford.

NDM Research Building, Oxford OX3 7FZ, UK.

chris.pugh@ndm.ox.ac.uk 44-1865-613961

* These authors made comparable contributions, AY initiated the experimental work and remained involved throughout; JH contributed essential immunological expertise in defining the immunological phenotype. AY is named first because his contributions were made over a longer period than those of JH.

** Joint senior authors; PJR and CWP initiated the project; CWP managed the project throughout; FI contributed essential immunological expertise.

*** Corresponding author

Author affiliations

1. Nuffield Department of Medicine, University of Oxford.
   NDM Research Building, Oxford OX3 7FZ, UK.
2. Transplantation Research Immunology Group, Nuffield Department of Surgical Sciences, University of Oxford.
   Level 6, John Radcliffe Hospital, Oxford OX3 9DU, UK.
3. Wellcome Trust Centre for Human Genetics, University of Oxford.
   Wellcome Trust Centre for Human Genetics, Oxford OX3 7BN, UK.
4. Nuffield Department of Medicine, University of Oxford.
   Henry Wellcome Building for Molecular Physiology, Oxford OX3 7BN, UK.
5. Now at
   Institute of Cancer and Genomic Sciences, University of Birmingham.
   IBR West Level 2, College of Medical and Dental Sciences,
   Edgbaston, Birmingham, B15 2TT, UK
6. Sandra and Edward Meyer Cancer Center, Weill Cornell Medicine, New York.

Department of Biochemistry, Weill Cornell Medicine, New York, NY 10021, USA.

7. Department of Cellular Pathology, Imperial College London.

   Imperial College London, London W2 1NY, UK.

8. MRC Centre for Regenerative Medicine, University of Edinburgh.

   MRC Centre for Regenerative Medicine, Edinburgh EH16 4UU, UK.

   Now at

   Barts Cancer Institute, Queen Mary University of London.

   Charterhouse Square, London EC1M 6BQ, UK.

9. Ludwig Institute for Cancer Research, Nuffield Department of Medicine, University of Oxford.

   Old Road Campus Research Building, Oxford OX3 7DQ, UK.

10. Veterinary Pathology, MRC Harwell.

    Mary Lyon Centre, Harwell Campus, Oxford OX11 0RD, UK.

11. Department of Pathology, University of Cambridge.

    Department of Pathology, Tennis Court Road, Cambridge, CB2 1QP, UK.

12. The Francis Crick Institute.

    1, Midland Road, London NW1 1AT, UK.

CONFLICT OF INTERESTS

PJR and CWP are scientific co-founders of ReOx Ltd, an Oxford University spin-out company interested in the development of drugs that target the HIF pathway; PJR has served on the Research Advisory Board of GlaxoSmithKline. CWP is a scientific co-founder of OxeHealth, an Oxford University spin-out company interested in non-contact patient monitoring. LED is a consultant and scientific advisory board member of Mirimus Inc. who has licensed aspects of in vivo shRNA technology that are employed in this work.

The other authors have declared that no conflicts of interest exist.

ABSTRACT

Physiological effects of cellular hypoxia are sensed by prolyl hydroxylase (PHD) enzymes which regulate HIFs. Genetic interventions on HIF/PHD pathways reveal multiple phenotypes that extend the known biology of hypoxia. Recent studies unexpectedly implicate HIF in aspects of multiple immune and inflammatory pathways. However, such studies are often limited by systemic lethal effects and/or use tissue-specific recombination systems, which are inherently irreversible, un-physiologically restricted and difficult to time. To study these processes better we developed recombinant mice which express tetracycline-regulated shRNAs broadly targeting the main components of the HIF/PHD pathway, permitting timed bi-directional intervention. We have shown that stabilization of HIF levels in adult mice through PHD2 enzyme silencing by RNA interference, or inducible recombination of floxed alleles, results in multi-lineage leukocytosis and features of autoimmunity. This phenotype was rapidly normalized on re-establishment of the hypoxia-sensing machinery when shRNA expression was discontinued. In both situations these effects were mediated principally through the *Hif2a* isoform. Assessment of cells bearing regulatory T cell markers from these mice revealed defective function and pro-inflammatory effects *in vivo*. We believe our findings have shown a new role for the *PHD2*/*Hif2a* couple in the reversible regulation of T cell and immune activity.

INTRODUCTION

Hypoxia-Inducible Factors (HIFs) are transcription factors composed of one of three alpha chains (HIF1α, HIF2α and HIF3α) dimerized to a beta chain that mediate the transcriptional response to low oxygen tensions (hypoxia). These HIF isoforms transduce different components of the hypoxia response, HIF1α and HIF2α being the most widely expressed and best understood. In the presence of oxygen, HIFα proteins are hydroxylated by prolyl hydroxylase domain (PHD) enzymes, leading to their recognition and destruction by the von Hippel Lindau (VHL) E3 ubiquitin ligase–proteasome pathway (1-4). Three closely related PHD enzymes have been identified, PHD1, PHD2 and PHD3, with PHD2 the most ubiquitous and most important at regulating HIF levels. Inhibition of PHD enzyme activity by low oxygen levels, or other means, leads to HIF activation. Together, the different HIF isoforms activate a wide range of transcriptional targets with established effects on angiogenesis, erythropoiesis and metabolism (1-4). It is increasingly clear that the HIF pathway also influences a number of other processes less directly related to oxygen homeostasis (5, 6). Immune and inflammatory pathways are of particular interest because of their central importance in disease. HIFs are widely expressed in leukocytes and in different settings have been reported to affect cell differentiation, migration, metabolism, growth, and apoptosis (7); as well as mediating changes in barrier function (8). Oxygen levels vary across the tissues in health (9) and in inflamed tissues hypoxia is generated by a combination of reduced oxygen availability, increased metabolic demands of rapidly-dividing and migrating leukocytes, and specific oxygen-consuming processes such as the respiratory (oxidative) burst (7). The effects of HIF pathway activation on immune and inflammatory pathways are therefore now of major medical importance, firstly because tissue hypoxia complicates most human diseases (10) and secondly, because drugs that target this pathway are now being tested in clinical trials (11).

Several studies have attempted to define physiological or pathological activities of the HIF/PHD system using genetic inactivation. At the level of the whole animal germ-line disruption of *Phd2* results in developmental defects and embryonic lethality, whilst conditional knockout of *Phd2* induced systemically in adult life leads to increased angiogenesis, erythrocytosis and changes in energy metabolism with ultimately lethal

consequences (12-15). Effects on the immune system from such global interventions have not been reported to date, perhaps because they have been obscured by these other phenotypes. In contrast, several studies have assessed the effects of targeting HIF/PHD pathway components in individual leukocyte subsets. For instance, major effects of HIF1α on innate cells, $CD4^+$ and $CD8^+$ T cells, T helper 17 (Th17) cells and regulatory T cells (Tregs) have been reported (16-34). Whilst these experiments have undoubtedly revealed an important role of the HIF/PHD system in immune function, the results reported have not always been congruent. Differences potentially arise because experiments that use lineage specific promoter driven knockout models (where genetic changes are activated only in specific cell populations at particular stages during development/cell differentiation) may fail to capture the complexity of natural immune cell interactions and entrain the risk of conflating adaptive physiology with developmental effects.

We chose to investigate the HIF pathway using inducible RNA interference gene knockdown *in vivo*. This offers the advantages of timed and reversible specific gene silencing in mature cells, producing effects potentially more analogous to those which might occur physiologically, pathologically or in response to pharmacological inhibition. In this study, we investigated the effects of intervention on the major HIF hydroxylase PHD2, with and without combined interventions on the two major HIF isoforms, HIF1α and HIF2α. We show that knockdown of *Phd2* mRNA in mice results in multi-lineage leukocytosis and immune dysregulation with features of autoimmunity which is at least partially dependent on changes in the behavior of cells bearing Treg markers. This phenotype is abrogated by simultaneous knockdown of *Hif2a* but not *Hif1a* mRNA.

RESULTS

Inducible shRNA knockdown

To explore the consequences of HIF pathway component suppression on normal mouse tissues, we developed transgenic inducible shRNA mice (Supplementary Figure 1A). Ten different shRNA sequences for *Phd2*, and five sequences for each of *Hif1a* and *Hif2a*, were tested initially for their effectiveness in reducing target gene mRNA levels following constitutive expression in mouse embryonic fibroblasts (Supplementary Table 1). For each target, the two sequences causing the greatest percentage reduction in target gene mRNA level were selected for further study (*Phd2#9, Phd2#3; Hif1a#5, Hif1a#1; Hif2a#3, Hif2a#1*). KH2 mouse embryonic stem (ES) cells expressing both a reverse tetracycline transactivator (*rtTA*) driven by the endogenous *GT(ROSA)26Sor* promoter *(R26*-rtTA) and a single copy tetracycline response element (*TRE*) controlled *GFP-shRNA* cassette (*TRE-shRNA*) bearing the relevant shRNA sequence downstream of the collagen type I gene (*Col1a1*), were generated using recombinase-mediated cassette exchange (RMCE) (35). Efficacy in this context was confirmed by culturing the cells on gelatin in the presence of doxycycline prior to assessing effects on target gene mRNA and protein levels, as well as downstream transcriptional effects (Supplementary Table 1; Supplementary Figure 1B). Following validation, ES cell clones were used to generate transgenic mice by blastocyst injection. Pure lines were then derived from the resultant chimeras and back-crossed to wild-type C57BL/6 mice for at least six generations prior to use.

Using these mice, we examined the consequences of sustained *Phd2* knockdown in adult mouse tissues by initiating *Phd2* silencing in 7-12 week-old mice. In order to increase the efficiency of Phd2 silencing, we generated shPhd2#9 and shPhd2#3 mice by crossing the respective *TRE-Phd2* alleles to mice harboring a transgene encoded at the *GT(ROSA)26Sor* locus that utilizes the strong exogenous *cytomegalovirus early enhancer element* and *chicken β-actin* (*CAG*) promoter to express a third-generation reverse tetracycline-regulated transactivator gene (*CAG-rtTA3*). This produces stronger and more ubiquitous target gene knockdown than observed when using *R26-rtTA* (35). Following treatment with doxycycline, these inducible shPhd2#9 mice showed widespread expression of GFP translated from the targeting sequence in all organs

examined when viewed at the whole tissue level (Supplementary Figure 1C). RT-PCR analysis showed that the shRNA sequence in these mice was effective at knocking down *Phd2* mRNA levels in all tissues (Supplementary Figure 1D). Although the size of effect varied somewhat between tissues, in all cases the degree of *Phd2* knockdown was sufficient to result in upregulation of *Phd3* and *Bnip3*, two HIF target genes, but had no consistent effect on *Actb* (*bActin*, a gene not considered to be a HIF target) (Supplementary Figure 1D). In keeping with these results, immunoblotting of liver extracts from doxycycline treated shPhd2#9 mice showed reduction in PHD2 protein levels and stabilization of HIF1α and HIF2α proteins (Supplementary Figure 1E). When doxycycline was removed, expression of GFP disappeared and *Phd2* mRNA levels normalized over two weeks (Supplementary Figure 1F). Equivalent results were obtained with the shPhd2#3 mice. Overall, the shPhd2 mice we have generated demonstrate effective, but reversible knockdown of *Phd2* mRNA across many tissues that is sufficient to stabilize/activate HIF and induce its target genes.

Long-term *Phd2* knockdown results in widespread leukocytosis and immune pathology

On treatment for 5-8 weeks with doxycycline, shPhd2#9 mice became unwell with weight loss, mild alopecia and greasiness of the remaining hair (Figure 1A). Control mice bearing the *CAG-rtTA* but not the tetracycline-responsive element *TRE-Phd2* shRNA allele remained healthy with doxycycline treatment. We were surprised to find that shPhd2#9 mice were anemic (haematocrit 36-38% compared with control levels of 51-55%) and had gross peripheral lymphadenopathy and splenomegaly (Figures 1B-C), although the mesenteric lymph nodes appeared macroscopically unremarkable.

Histological examination confirmed the expansion of lymphoid tissues with distortion of the normal architecture, but with no features suggestive of neoplastic transformation (Figure 1D). Eosinophilic mononuclear cells were prominent, expanding the central regions of lymph nodes and displacing cortical areas to the extreme periphery (Figure 1D-G); similar changes were seen in the splenic white pulp (Figure 1H-I). Examination of the skin of the pinna showed thickening of both epidermis and dermis with loss of subcutaneous fat. There was a diffuse lymphohistiocytic infiltrate within the dermis and evidence of exocytosis of lymphocytes into the epidermis (Figure 1J-L). Elsewhere, empty hair follicles were detected.

Examination of other tissues revealed further changes, with striking perivascular accumulations of leukocytes in the bronchovascular regions of the lung (Figure 1M) and accumulations in the kidney (Figure 1N), similar to those seen in some human autoimmune diseases. Further examination of the kidney showed an increase in glomerular size with endocapillary hypercellularity indicative of a nephritis (Figure 1O-P); there was no tubulointerstitial inflammation. In the liver, steatosis was apparent and smaller collections of leukocytes were seen in both periportal and perivenous sites (Figure 1Q). Patchy infiltration by leukocytes was also found in the epicardium (Figure 1R) and scattered throughout skeletal muscle. Lymphoid aggregates can be seen as background changes in various organs in some mouse colonies, but in mice from this laboratory aggregates were consistently more prominent in the shPhd2#9 than control mice. Similar lymphadenopathy and splenomegaly with multi-lineage changes and comparable histological changes were observed with the shPhd2#3 mice that bear an independent sequence targeting *Phd2* (Supplementary Figure 2).

In a subsequent experiment we monitored body weight and haematological parameters during an 8-week period of *Phd2* knockdown. Differences in body weight of knockdown mice compared to control mice began to be apparent after two weeks and were progressive (Supplementary Figure 3A). We observed the expected rise in red cell count over the first two weeks, but thereafter the red cell count fell (Supplementary Figure 3B). There was a progressive rise in leukocyte counts throughout the period and platelet counts were also higher in shPhd2#9 mice than in control animals (Supplementary Figures 3C-D). Anti-nuclear antibodies could be detected in serum within the first three weeks of treatment.

Immunological effects observed in shPhd2 mice are multi-lineage and *Hif2a* isoform-dependent

Flow cytometric analysis revealed that the lymphadenopathy was arising from effects across multiple leukocyte lineages; total leukocytes, T cells, B cells and myeloid lineages as defined by CD45, CD3, B220 and GR1 (Ly-6G/Ly-6C) positivity (Figure 2A; Supplementary Figure 4A). We next sought to determine whether these immunological effects were present, although previously unreported, in conditional *Phd2* knockout animals. We examined mice bearing a tamoxifen-inducible Cre recombinase expressing transgene (*Rosa26Cre*^{ERT2}) that were homozygous for floxed *Phd2* alleles (*Rosa*ERT*Cre*;*Phd2*fl/fl) four weeks after

tamoxifen treatment. Peripheral lymphadenopathy was present in both knockdown and knockout models (Figures 2B, E) as was the leukocyte expansion (Figures 2A, D).

Next, in order to assess whether the phenotype was dependent specifically on the up-regulation of either HIFα isoform, we developed double knockdown and double knockout mice in which both *Phd2* and *Hif1a* or *Hif2a* were targeted. shPhd2Hif1 and shPhd2Hif2 mice all carried one *CAG-rtTA3* allele, one *TRE-Phd2#9* and a *TRE-Hif* allele targeting *Hif1a* or *Hif2a* respectively. shPhd2Hif1 and shPhd2Hif2 mice were treated with doxycycline at a dose of 2 mg/ml in their drinking water for four weeks before analysis. The efficacy and specificity of *Hif1a* and *Hif2a* knockdown at the mRNA level in liver and spleen is shown in Supplementary Figure 5. Phd2Hif1ko and Phd2Hif2ko mice all carried one *Rosa26Cre*^{ERT2} allele, were homozygous for floxed *Phd2* alleles and homozygous for floxed alleles of *Hif1a* or *Hif2a* respectively. Phd2Hif1ko and Phd2Hif2ko mice were examined four weeks after being treated with tamoxifen by gavage. In each model, the phenotype was reversed by concomitant *Hif2a* knockdown or knockout respectively (Figures 2B-C, E). Additionally, expansion of all leukocyte lineages was completely ameliorated by concomitant HIF2α deficiency and partially reversed by concomitant HIF1α deficiency (Figures 2A, D). Similarly, the inflammatory histological changes with *Phd2* knockdown were abrogated with concomitant HIF2α but not HIF1α deficiency (Figure 3).

In summary, the major features of the shPhd2 phenotype are of *Hif2a*-dependent lymphadenopathy, multi-lineage leukocytosis, weight loss, anti-nuclear antibody development and immune-mediated organ pathology. These features are also seen in Phd2ko animals.

Reversibility of the shPhd2 phenotype

We next explored the reversibility of the observed phenotype on re-expression of *Phd2* following doxycycline withdrawal. Groups of animals were treated with doxycycline for 3-4 weeks until the first members of each test cohort began to become unwell as described above, triggering examination of tissues and serum from a randomly selected subset of the animals. The remaining animals were taken off doxycycline, their weight was monitored and tissues and serum were subsequently examined. The animals treated with doxycycline lost

weight, developed lymphadenopathy with expansion of all lineages, serum became positive for anti-nuclear antibodies and histological examination confirmed the previously described changes (Figure 4). Following doxycycline withdrawal, the lymphadenopathy regressed (Figure 4A), the mice regained weight (Figure 4B), the anti-nuclear antibodies disappeared (Figure 4C) and the histological and immunological features improved (Figures 4D-L). This indicates that the changes observed in shPhd2 mice are reversible and not due to either a permanent change in cell phenotype or irrevocable loss of cells with a particular function.

The shPhd2 phenotype is transferrable by bone marrow transplantation

The phenotype observed has many features suggestive of autoimmune disease but since the reduction of expression of *Phd2* in these mice was systemic, it was unclear whether this phenotype could arise purely through effects on the immune system. To test the role of the immune system in this phenotype we next created bone marrow chimeras bearing shPhd2 bone marrow in the context of an otherwise normal animal. A congenic recipient strain (CD45.1) was used to confirm complete reconstitution with donor leukocytes. Control mice were generated in parallel that received bone marrow from mice carrying the *CAG-rtTA* allele but not the *TRE-Phd2* shRNA targeting sequence. Bone marrow was allowed to engraft for 8 weeks following transplantation prior to treatment with doxycycline. On treatment with doxycycline, recipients of knockdown bone marrow (BMT-shPhd2#9), but not control bone marrow (BMT-Ctrl), developed lymph node enlargement with multi-lineage expansion and detectable anti-nuclear antibodies in their serum (Figure 5A-C), although skin changes and tissue infiltration were less prominent than in the previous experiments (Figure 5D-G). In both groups of animals, leukocytes in the peripheral blood were all of donor type (as defined by the *Ptprc*^{a} pan-leukocyte marker CD45.2) at the points of analysis. This indicates that when *Phd2* knockdown is restricted to the bone marrow this is sufficient to generate the major features of the phenotype seen in shPhd2 mice.

Phd2 knockdown produces features of immune dysregulation

Taken together these features suggested that the overall phenotype in shPhd2 mice was being driven, at least in part, by immune dysregulation. We therefore examined these mice for the presence of cells bearing

T cell subset markers relating to helper, effector and regulatory functions. Examination of expression of CD4 and CD8 revealed an increase in the absolute numbers of $CD4^+CD8^-$ and $CD4^-CD8^+$ cells in lymph nodes from shPhd2#9 mice compared with control mice following 4 weeks doxycycline treatment (Figure 6A; Supplementary Figure 4B). Although the absolute numbers of these cell populations changed, their representation when considered as a percentage of total $CD3^+$ cells was relatively constant (Figure 6A). The absolute numbers of double positive and double negative cells remained low (Figure 6A, Supplementary Figure 6A). We next went on to examine cells expressing CD25 and Foxp3, markers normally associated with regulatory T cell function, within the $CD4^+$ population. Given the immune dysregulation in these mice we were surprised to find that shPhd2 mice (with either targeting sequence) showed increased absolute numbers of $CD4^+CD25^+Foxp3^+$ T cells in peripheral lymph nodes (Figure 6B). $Foxp3^+$ cells were also more abundant in spleen and bone marrow, although some of these cells no longer expressed CD25 (Supplementary Figure 6B-C). The relative abundance of Foxp3+ cells as a proportion of $CD4^+$ T cell populations was also increased (Figure 6B; Supplementary Figure 6B). Increased $Foxp3^+$ counts were also seen in the lymph nodes of recipients of knockdown, but not control, bone marrow, indicating that it was a marrow endogenous function and not a response to non-immune abnormalities caused by widespread PHD2 deficiency (Figure 6C). The increase in $Foxp3^+$ counts was reversible on doxycycline withdrawal (Figure 6D). In keeping with the overall phenotype, the increase in number of $Foxp3^+$ cells was totally corrected by simultaneous *Hif2a* deficiency and partially reduced by *Hif1a* deficiency in the doxycycline-treated shPhd2 mice and *Phd2* knockout (Phd2ko) animals (Figure 6E-F). Similar trends were found in lymph nodes and bone marrow, but not the spleen, of *Phd2* knockout (Phd2ko) animals (Figure 6F; Supplementary Figure 6D). The Treg-specific demethylated region (TSDR) was demethylated in $Foxp3^+$ cells isolated from doxycycline-treated shPhd2 mice (Figure 6G).

Given the paradox of increased numbers of cells bearing regulatory T cell markers in mice with an autoimmune phenotype, we next tested the function of these cells. The ability of $CD4^+CD25^+$ cells to regulate the activity of effector cells in skin allograft rejection *in vivo* was assessed (Figure 7A). Immunodeficient C57BL/6 ($H\text{-}2^b$) $Rag1^{-/-}$ mice were reconstituted with $CD4^+CD25^-$ effector T cells from wild-type C57BL/6 (H-

2^b) mice, either alone or in combination with shPhd2 or control $CD4^+CD25^+$ 'Tregs' (expressing Foxp3 at >85% purity, using previously established cell doses (36)) and subsequently received a CBA (H-2^k) skin transplant. shPhd2 $CD4^+CD25^+$ cells were isolated from mice carrying both *CAG-rtTA* and *TRE-Phd2* shRNA alleles, whereas control $CD4^+CD25^+$ cells were isolated from mice carrying the *CAG-rtTA* allele alone. In initial experiments, $CD4^+CD25^+$ cells were derived from donor animals pre-treated with doxycycline to ensure any change in function resulting from Phd2 knockdown had already developed (Figure 7B) and doxycycline treatment was continued for the duration of the experiment post-transplantation to ensure that Phd2 knockdown was maintained. In these experiments we observed that $CD4^+CD25^+$ cells from doxycycline pre-treated shRNA mice were unable to control skin rejection to the same degree as control $CD4^+CD25^+$ cells.

In subsequent experiments, cells were obtained from mice of the same genotypes but doxycycline treatment was only started after adoptive transfer into the recipient mice to ensure that the effects of Phd2 knockdown were being tested on cell subsets that were identical at the point of transfer into the C57BL/6 (H-2^b) $Rag1^{-/-}$ recipients. Again, in contrast to the $CD4^+CD25^+$ cells from mice carrying the *CAG-rtTA* allele alone, shPhd2 $CD4^+CD25^+$ cells were unable to control graft rejection (Figure 7C). In both assays, shPhd2 $CD4^+CD25^+$ cells provided no quantifiable benefit to graft survival, with grafts being rejected at least as fast as in mice receiving effector cells alone, indicating total loss of regulatory function in this *in vivo* model.

In parallel, *in vitro* experiments were performed to assess the ability of doxycycline treated $CD4^+CD25^+$ cells, from the same sources, to suppress the proliferation of $CD4^+CD25^-$ responder cells stimulated either polyclonally with anti-CD3/anti-CD28 beads or with allogeneic dendritic cells (DCs) (Figure 7D). In both assays (Figures 7E and F respectively) $CD4^+CD25^+$ cells from doxycycline-treated shPhd2 animals were less effective at regulating the proliferative response than those from control animals. Taken together, the results of both *in vivo* and *in vitro* experiments indicate that $CD4^+CD25^+$ cells are hypofunctional as immune regulators when *Phd2* levels are knocked down, suggesting that deficiency of regulatory T cell function may contribute to the autoimmune phenotype we have observed.

Noting that skin graft rejection appeared slightly faster in the presence of $CD4^+CD25^+$ shPhd2 cells than when effector cells were present alone, we tested the ability of $CD4^+CD25^+$ shPhd2 cells to reject a skin graft in isolation (Figure 8A). Intriguingly, cells selected with this surface phenotype prior to doxycycline treatment and then adoptively transferred into $Rag1^{-/-}$ recipients were able to reject skin allografts when these mice were treated with doxycycline whereas we observed long-term graft survival in the doxycycline-treated recipients of $CD4^+CD25^+$ cells from control mice (Figure 8B). This indicates that Phd2 knockdown may lead to a converse effector function in this population of cells. Additionally, the shPhd2 recipient mice, but not those receiving control cells, developed features of the phenotype observed in shPhd2 mice, becoming unwell and losing weight and leading to early termination of the experiment in one animal. The loss of regulatory function and/or conversion to effector functionality can therefore induce the development of an autoimmune phenotype in shPhd2 mice.

To analyse the basis for these functional differences we compared the expression of key transcription factors and cytokines in $CD4^+Foxp3^+$ and $CD4^+Foxp3^-$ cells from shPhd2 and control mice (Figure 9; Supplementary Figure 7). We show that despite on-going expression of Foxp3 cells within this population from shPhd2 mice expressed increased levels of Tbet and TNFα, but not IFNγ, RORγt, GATA-3, IL-2, -4, - 10 or -17. To take this analysis further we examined the expression of CD44 and CD62L in $CD4^+Foxp3^+$ and $CD4^+Foxp3^-$ cells from shPhd2 and control mice, showing that in both populations Phd2kd leads to a reduction in cells with a $CD44^{lo}CD62L^{hi}$ ‘naïve’ phenotype and an increase in $CD44^{hi}CD62L^{lo}$ ‘effector memory’ cells (Figure 10; Supplementary Figure 8).

DISCUSSION

Here we report on a new model for the genetic investigation of HIF-PHD hypoxia signalling pathways in the mouse, and on the occurrence of a systemic autoimmune phenotype following suppression of the principal HIF prolyl hydroxylase, PHD2. Following shRNA-mediated knockdown of *Phd2*, mice developed a multi-lineage leukocyte expansion, associated with destruction of lymphoid organ architecture, immune infiltration of major organs, and anti-nuclear antibodies. In keeping with the stochastic nature of immune responses this phenotype was somewhat variable between individual knockdown mice, but overall the phenotype was transferrable by bone marrow transplantation, and reversible when doxycycline-driven shRNA-mediated suppression of *Phd2* was stopped.

These findings strongly suggested the occurrence of an autoimmune syndrome, but were somewhat surprising in view of early reports on general inactivation of *Phd2* using conditionally activated Cre recombinase, which did not highlight such a phenotype. Nevertheless, near identical phenotypes obtained using two distinct shRNAs and complete suppression by co-incident shRNA-mediated knockdown of *Hif2α*, strongly suggested that the phenotype reflected 'on-target' actions of the interventions. We therefore re-examined the phenotype of Cre-recombinase mediated *Phd2* inactivation in a further set of mice. These experiments revealed a similar, though somewhat less severe, inflammatory phenotype associated with development of anti-nuclear antibodies, which was also suppressed by combined inactivation of *Phd2* with *Hif2α*. Though it is possible that this phenotype was obscured in the earlier studies by other, ultimately fatal, consequences of *Phd2* inactivation, we note that one of the earlier reports of *Phd2* knockout mice records the occurrence of leukocytosis and thrombocytosis such as we observed in the present study (14). Taken together our findings indicate that *Phd2* knockdown or knockout, in adult mice, has the potential to cause an autoimmune phenotype driven by cells originating within the bone marrow.

We are unclear why this phenotype was generally stronger in the knockdown than the knockout animals, although we cannot exclude a sensitizing effect of RNA interference or doxycycline. However, no such effects have been described in multiple reports of the use of the same doxycycline-inducible shRNA system to target

other genes (37-40). Other important differences between the knockdown and knockout systems could be relevant. In our experience, recombination between the loxP sites in the conditional Phd2 knockout allele was always less than complete in any cell population within the *Rosa-CreER* knockout (Phd2ko) mice that we deployed. Thus, it could be that residual, normal un-recombined cells were sufficient to significantly suppress the phenotype, whereas in the knockdown system all cells would be expected to be affected by the shRNA expression, thus no potentially compensatory normal cells would be present. Equally, it is possible that complete knockout of *Phd2* in certain cells leads to their deletion, and hence a phenotype that is somewhat less severe. Whatever the explanation for these quantitative differences, the occurrence of a qualitatively similar phenotype was reproducible across the two models, and therefore potentially relevant both to the physiology of immune regulation, and to the clinical development of PHD2 and HIF2α inhibitors.

Tregs, which express the forkhead box transcription factor Foxp3, are key to immune homeostasis, and their disruption results in pathology with a number of similarities to those that we observed in shPhd2 mice. Scurfy mice have a disabling mutation of Foxp3, which leads to a fatal lymphoproliferative disorder (41). Human mutations in the *FOXP3* gene cause an X-linked syndrome (IPEX) characterized by immune dysregulation, polyendocrinopathy and enteropathy (42, 43). Although it is formally possible that the development of anti-nuclear autoantibodies in our model was simply a consequence of the expansion of the total number of B cells, similarities in the lymphoid pathology of these conditions to that observed in shPhd2 mice led us to examine 'Tregs' (cells bearing regulatory T cell markers ($CD4^+CD25^+$ and/or $Foxp3^+$) from shPhd2 mice) from these mice further. In contrast to most other models of immune dysregulation we found that the absolute number of these 'Tregs' in shPhd2 mice was increased compared with controls and their ratio relative to the cell populations they control was also increased in the lymph nodes, but not in the spleen. However, when equal numbers of cells are directly compared the ability of 'Tregs' (as defined by the expression of these markers) from shPhd2 animals to suppress either skin allograft rejection, or *in vitro* responder T cell proliferation, was impaired. The TSDR within the Foxp3 locus of shPhd2-derived $CD4^+CD25^+$ cells remained demethylated. Since expression of Foxp3 is dependent on selective demethylation of the TSDR (44), this finding is consistent with the maintained expression of Foxp3 observed. Furthermore, the absence of

epigenetic changes is consistent with the reversible nature of the phenotype on doxycyline withdrawal in shPhd2 mice, which is relatively rapid in relation to the normal life-span of regulatory T cells. Phenotypically, these cells increased their expression of Tbet and TNFα and gained a $CD44^{hi}CD62L^{lo}$ effector memory phenotype, but did not manifest features of Th17 conversion. Taken together these results suggest that there is a functional switch downstream of, or independent from, Foxp3. However, this change is not simply a loss of regulatory function since shPhd2 knockdown, induced after cells expressing regulatory T cell markers were transferred into an immunodeficient recipient, results in cells being present that act positively to cause skin allograft rejection in the absence of any other effector population, indicating that a functional inversion had occurred within the transferred population.

Several studies have reported on abnormalities in lymphocyte differentiation following genetic interventions on HIF or its regulatory machinery, in specific subsets of lymphocytes (16-31, 33). These phenotypes include abnormalities of regulatory T cells in some studies, but the results were not always concordant and differ from our current findings. For instance, inactivation of *Vhl*, the gene encoding the ubiquitin E3 ligase that targets hydroxylated HIFα polypeptides for proteasomal destruction, using Cre-recombinase restricted by a *Foxp3* promoter, resulted in a reduction of Foxp3 expression and an inflammatory phenotype that was dependent on HIF1α (29).

Our studies in the new model are the first to interrogate T cell function in the setting of general inactivation of *Phd2*, a difference which is likely important in view of the potential for cross-talk between subsets of lymphocytes. The observation of cells bearing classical regulatory T cell markers, which were apparently hypofunctional in immune suppression, or even stimulatory is unusual. Nevertheless, the results are consistent with emerging data on functional heterogeneity in regulatory T cells. For instance, it is increasingly clear that Foxp3 alone does not ensure stability of the suppressive function of regulatory T cells (45, 46). A number of additional factors are important for this function, including signalling through the TCR and CD25 (47, 48), and other signaling pathways such as Nrp1 (33, 49), Foxo1/3a (50) and Eos (51). Furthermore, the multi-functional potential of regulatory T cells is increasingly thought to be required physiologically for

specific responses that are dependent on micro-environmental cues (46, 52-55). Environmental cues identified to date include the presence of Toll-like receptor ligands or inflammatory cytokines such as IL-1β and IL-6 (56-58). Local tissue hypoxia is an established consequence of inflammation and our results suggest a mechanism by which, in this setting, hypoxia may provide an additional cue for regulatory T cells to modify their behavior and assist in the potentiation of required immune responses.

Inhibitors of PHD2 are now undergoing late-phase clinical trials for the treatment of anemia in patients with kidney diseases (59). In this setting, very low intermittent dosing schedules are used in an attempt to specifically target the erythropoietin production in the diseased kidneys and liver. This contrasts with our use of high dose doxycycline and widely expressed transgene promoters to knockdown or knockout PHD2, so that it is unlikely that exposures to the interventions are equivalent. In preliminary studies we have not observed consistent effects of prolyl hydroxylase inhibitors on human Tregs, using short-term (≤72 hours) treatment of isolated cells. Nevertheless, we consider that awareness of our findings is important. Interestingly, the anti-hypertensive agent hydralazine has inhibitory action against the HIF hydroxylases (60), and causes 'drug-induced' systemic lupus erythematosus in a dose dependent manner (61). Importantly the syndrome we describe, and hydralazine-induced lupus, are both reversible. Thus, attempts to enhance immunity by PHD2 inhibition in specific settings might be a clinically credible strategy meriting assessment in future studies. Our finding that the autoimmune syndrome was suppressed by concurrent knockdown of *Hif2a* also suggests that the newly developed HIF2α antagonists, currently in clinical trials for renal cancer (62), might be assessed in autoimmunity and transplantation. Overall, our newly-developed model for reversible intervention on the HIF-PHD system, and the findings we believe to be novel on dysregulation of immune function should be of interest as this emerging area of medicine is explored.

METHODS

Constructs and shRNAs

miR30-based shRNA targeting vectors were cloned as previously described (35, 63). To identify potent shRNAs targeting murine *Phd2*, multiple 97-bp oligonucleotides (x10) predicted from shRNA design algorithms (35) were XhoI-EcoRI cloned into the miR-30 cassette of the pGIPZ vector and screened for effects on mRNA levels in mouse embryonic fibroblasts (MEFs) using qPCR. Sequences were introduced by lentiviral infection into MEFs and after 48 hours of doxycycline (Dox; Doxycycline hyclate) treatment (2μg/ml) target gene mRNA levels were measured, normalized against *Actb* and percentage knockdown in transgenic cells was compared with control cells which received an shRNA against *Firefly-Luciferase* (Supplementary Table 1). For knockdown of murine *Hif1a* and *Hif2a*, multiple shRNAs (x5 of each) were designed, cloned, and their knockdown levels tested as described above.

ES cell targeting and generation of transgenic mice

The targeting and screening strategy for embryonic stem (ES) cell production followed the method described previously (35, 63). Two potent shRNAs against murine *Phd2* (shPhd2#9 97-mer: 5'-TGCTGTTGACAGTGAGCGCCGCCACAAGGTACGCAATAACTAGTGAAGCCACAGATGTAGTTATTGCGTACCTTGTGGCGTTGCCTACTGCCTCGGA-3' and shPhd2#3 97-mer: 5'-TGCTGTTGACAGTGAGCGCACGCAATAACTGTTTGGTATTTAGTGAAGCCACAGATGTAAATACCAAACAGTTATTGCGTATGCCTACTGCCTCGGA-3') were cloned into a cassette that links EGFP and shRNA expression downstream of a *TRE*, and targeted by recombinase-mediated cassette exchange into a defined locus downstream of the collagen, type I, alpha 1 (*Col1a1*) gene in KH2 ES cells, which also express the reverse-transactivator (*rtTA*) from the *Gt(ROSA)26Sor* promoter (35, 63). Southern blotting demonstrated correct transgene insertion, and doxycycline-inducible knockdown of endogenous *Phd2* was confirmed by qPCR and immunoblot analysis. Germline transgenic mice were generated by the standard blastocyst-injection method. MEFs were generated from 13.5-day-old embryos according to standard protocols. A similar approach was adopted for the creation of knockdown mice targeting *Hif1a* and *Hif2a* (shHif1 and shHif2 mice respectively) using the

most efficient shRNAs identified in our preliminary screening (*shHif1a#5* 97-mer: 5'-TGCTGTTGACAGTGAGCGAACGGGCCATATTCATGTCTATTAGTGAAGCCACAGATGTAATAGACATGAATATGGCCC GTGTGCCTACTGCCTCGGA-3' and *shHif2a#3* 97-mer: 5'-TGCTGTTGACAGTGAGCGAACACTTGATGTGGAAACGTATTAGTGAAGCCACAGATGTAATACGTTTCCACATCAAGT GTGTGCCTACTGCCTCGGA-3').

Mice were subsequently inter-crossed with *CAG-rtTA* reverse-transactivator lines which were obtained from Jackson Laboratories (Maine, USA) to generate heterozygous double-transgenic (*CAG-rtTA+/-;TRE-shRNA+/-*) mice. Mice were back-crossed over six times with C57BL/6JOlaHsd wild-type mice (Envigo). *Phd2* single knockdown mice carried alleles of *CAG-rtTA+/-;TRE-shPhd2#9+/-* (shPhd2#9) or *CAG-rtTA+/-;TRE-shPhd2#3+/-* (shPhd2#3). Control mouse lines for knockdown experiments carried a single allele of *CAG-rtTA* but no *TRE* allele (*CAG-rtTA+/-;TRE-/-*) (Ctrl). For double knockdown mice bearing both *Phd2* and *Hif1a* or *Hif2a* knockdown alleles, *CAG-rtTA+/+;TRE-shPhd2#9+/-* mice were crossed with *CAG-rtTA-/-;TRE-shHif1a#5+/-* or *CAG-rtTA-/-;TRE-shHif2a#3+/-* to produce *CAG-rtTA+/-;TRE-shPhd2#9+/TRE-shHif1a#5+* (shPhd2Hif1) or *CAG-rtTA+/-;TRE-shPhd2#9+/TRE-shHif2a#3+* (shPhd2Hif2) mice. To induce shRNA expression, shRNA mice and control mice were provided with *ad libitum* access to drinking-water containing 2mg/mL of doxycycline with 30% sucrose from the age of 8-12 weeks. All knockout mouse lines listed below were also bred in our facilities: *RosaERTCre;Phd2fl/fl* (Phd2ko), *RosaERTCre;Phd2fl/fl;HIf1afl/fl* (Phd2Hif1ko), *RosaERTCre;Phd2fl/fl;HIf2afl/fl* (Phd2Hif2ko), and *RosaERTCre;-* (control, Ctrl) mice and have been described before (64). Tissues from knockout and control mice were harvested four weeks after receiving Tamoxifen treatment for one week by oral gavage. All knockdown and knockout mouse lines were housed in the Functional Genetics Facility of the Wellcome Trust Centre for Human Genetics (University of Oxford, UK) in individually ventilated cages, with the only reported positives on health screening over the entire time course of these studies being for *Helicobacter* spp, *Tritrichomonas* spp and *Entamoeba* spp. Food and water was provided *ad libitum* and animals were maintained on a 12 hour light/dark cycle. After the preliminary experiments subsequent phenotyping experiments were blinded and randomized as indicated and no animals were excluded from the study.

Characterization of transgenic shRNA mice

Brightfield images and GFP expression were assessed in tissues obtained from shRNA Phd2 knockdown mice driven by *CAG-rtTA* and treated with doxycycline (2mg/ml drinking water with 30% sucrose *ad libitum*) for the period indicated in the figure legends, following fixation with fresh 10% neutral buffered formalin. Images were acquired using an image scanner (ChemiDoc™ XRS+ System with Image Lab™ Software, Bio-Rad Laboratories Ltd., Watford, Hertfordshire, UK).

Hematological analysis

Mice were culled and blood obtained from the inferior vena cava, or heart, was collected into heparin pre-filled tubes. Blood samples were immediately analyzed using a Sysmex KX-21N™ Automated Hematology Analyzer (Sysmex Corporation, Milton Keynes, Buckinghamshire, UK).

Anti-nuclear antibodies (ANA) tests

Mouse serum samples were diluted 10 times and added to slides pre-coated with human epithelial HEp-2 cells (Fluorescent ANA Test System, Immuno Concepts, Sacramento, California). These were then stained with a goat anti-mouse immunoglobulin G (IgG) Alexa Fluor 488 (Invitrogen, Carlsbad, California) secondary antibody (diluted 1:500 in phosphate-buffered saline (PBS)). Fluorescent images were acquired using a fluorescence stereomicroscope as described in (65).

Expression analysis

RNA was extracted from several mouse tissues using a TRI Reagent® (Sigma-Aldrich, Poole, Dorset, UK) or RNeasy kit (QIAGEN, Manchester, UK). Purified total RNA (0.5-1.0μg) was reverse-transcribed using an RT-PCR kit (High Capacity cDNA Reverse Transcription Kit, Applied Biosystems, Thermo Fisher, Waltham, Massachusetts). mRNA expression was determined by RT-qPCR (Platinum SYBR Green; Invitrogen, Carlsbad, California), using the primer pairs for *Phd2* (forward-GCCCAGTTTGCTGACATTGAAC and reverse-CCCTCACACCTTTCTCACCTGTTAG), *Hif1a* (forward-TGCTCATCAGTTGCCACTTCC and reverse-

CCATCTGTGCCTTCATCTCATCTTC), *Hif2a/EPAS1* (forward-ACGGAGGTCTTCTATGAGTTGGC and reverse-GTTATCCATTTGCTGGTCGGC), *Bnip3* (forward-GACGAAGTAGCTCCAAGAGTTCTCA and reverse-CTATTTCAGCTCTGTTGGTATCTTGTG), *Phd3* (forward-TCAACTTCCTCCTGTCCCTCATC and reverse-GCGAACATAACCTGTCCCATTTC), *Actb (β-actin)*, (forward-CTAGGCACCAGGGTGTGAT and reverse-TGCCAGATCTTCTCCATGTC), *Hprt* (forward-GTTGGATACAGGCCAGACTTT and reverse-CCACAGGACTAGAACTGC), *Egfp* (forward-TGCTCAGGTAGTGGTTGTCG and reverse-AGAACGGCATCAAGGTGAAC). Values were analyzed as "RQ" (Relative quantification=$2^{-\Delta\Delta Ct}$) against the expression levels of the house-keeping genes *Hprt* or *Actb (β-actin)* by Step One Plus Real-Time PCR System (Applied Biosystems, Thermo Fisher, Waltham, Massachusetts).

Western blotting, flow cytometry and antibodies

Western blotting was performed according to standard protocols in our laboratory (66). In brief, tissues were snap frozen in liquid nitrogen and homogenized using a glass-homogenizer on ice. Protein was extracted using a standard protein lysis buffer (10mM Tris (pH7.5), 1% SDS, 10% Glycerol, 6.87M Urea) supplemented with a protease inhibitor cocktail (Complete; Roche Diagnostics, Burgess Hill, W. Sussex, UK) and quantified using a Pierce™ BCA Protein Assay Kit (Thermo Fisher, Waltham, Massachusetts). Proteins were separated on a polyacrylamide gel (Tris-Glycine 8-16% mini, NuSep Inc., Generon, Maidenhead, Berkshire, UK) and transferred to a PVDF membrane (Immobilon-P (0.45μm), Millipore, Watford, Hertfordshire, UK). Primary antibodies used for Western blot analysis included those against PHD2 (NB100-2219, Novus Biologicals, Abingdon, Oxfordshire, UK), HIF1α (NB100-479, Novus Biologicals), HIF2α (NB100-122, Novus Biologicals), PHD3 (produced in our facility (66)), ACTB (ab49900, Abcam, Cambridge, UK) followed by HRP-conjugated secondary antibodies. Conversion of chemiluminescent substrate was measured on an Image scanner (ChemiDoc™ XRS+ System with Image Lab™ Software, Bio-Rad Laboratories Ltd., Watford, Hertfordshire, UK).

For flow cytometric analysis (FACS), single cell suspensions were prepared from peripheral lymph nodes (subiliac and axillary), spleen and femoral bone marrow in FACS-buffer (PBS, pH7.4, 1% BSA). Following red blood cell lysis, cells were stained with the indicated antibodies as per the manufacturer's protocol. Cell

preparations were stained with 7-AAD (eBioscience, Thermo Fisher, Waltham, Massachusetts) and only live cells were analyzed. After washing, cells were measured using a BD Canto II (BD Biosciences, Wokingham, Berkshire, UK) FACS machine and analyzed using DIVA followed by FlowJo software (Tree Star, Ashland, Oregon). For intracellular Foxp3 measurement, cells were fixed and permeabilized using a Foxp3 staining kit (eBioscience, Thermo Fisher, Waltham, Massachusetts) before staining for Foxp3 according to the manufacturer's protocol. The following antibodies were used for flow cytometry (clone; manufacturer): CD3 (145-2C11; eBioscience), CD3 (17A2; eBioscience), CD4 (GK1.5; eBioscience), CD8 (53-6.7; eBioscience), B220 (30-H12; eBioscience), CD45 (30-F11; eBioscience), CD19 (9B1; eBioscience), Gr-1 (RB6-8C5; eBioscience), CD25 (PC61; eBioscience), CD25 (PC61; BD Biosciences), Foxp3 (30-F11; eBioscience), Foxp3 (FJK-16s; eBioscience), CD62L (MEL-14; BD Biosciences), CD44 (IM7; Biolegend), IL-17A (ebio17B7; eBioscience), IL-4 (BVD6-24G2; eBioscience), IFN-γ (XMG1.2; eBioscience), IL-2 (JES6-5H4; eBioscience), TNF-α (MP6-XT22; eBioscience), IL-10 (JES5-16E3; eBioscience), GATA-3 (L50-823; BD Biosciences), T-bet (ebio4b10; eBioscience), and ROR-γt (AFKJS-9; eBioscience). The secretion of IL-17A, IL-4, IFN-γ, IL-2, TNF-α, and IL-10 was determined by flow cytometry after 5-hr stimulation with 1 μg/mL ionomycin (Sigma, cat. no. 56092-82-1), 100ng/mL PMA (Sigma, cat. no. P1585), and 5μg/mL Brefeldin A (Biolegend, cat. no. 420601). Gating strategies are shown in Supplementary Figure 4.

Histology

Organ samples were fixed in fresh 10% neutral buffered formalin (Sigma-Aldrich, Poole, Dorset, UK) overnight and further subjected to routine histological procedures for embedding in paraffin. 4μm sections from at least two or three different animals per group were placed on slides adjacent to each other to enable cross comparison within a slide after hematoxylin and eosin (H&E) staining. Whole tissue sections were scanned at x400 magnification using a NanoZoomer S210 digital slide scanner and reviewed using NDP.view2 software (Hamamatsu Photonics, Shizuoka, Japan). Tissues were initially analyzed and scored in a blinded fashion by an independent mouse histopathologist (CLS); representative images were subsequently chosen by PSM and AY to illustrate key histological findings.

Cell purification for adoptive transfer

$CD4^+CD25^+$ and $CD4^+CD25^{neg}$ cells were isolated using the Miltenyi MACS system (Miltenyi Biotec Ltd., Woking, Surrey, UK) as previously described (45). Single cell suspensions were prepared from lymph nodes and spleens of 8-12 week-old shPhd2#9, control (Ctrl) or wild-type C57BL/6 mice, red cells lysed, and cells re-suspended in PBS/1% fetal bovine serum (FBS). $2x10^8$ cells were then stained with rat anti-mouse antibodies against CD8 (clone YTS 169, 80μg), B220 (clone RA3-6B2, 100μg), MHC class II (clone TIB 120, 100μg) and Mac-1 (M1-70, 100μg) followed by magnetic negative depletion using sheep-anti-rat IgG-coated Dynabeads (Dynal Biotech, Thermo Fisher, Waltham, Massachusetts, 500μl of beads per $2x10^8$ cells). After magnetic separation, the remaining cells were stained with anti-CD25 phycoerythrin (PE) antibody (eBioscience, clone PC61.5; 5μl per 10^8 of initial cell number) and then with anti-PE microbeads (Miltenyi Biotec Ltd. Woking, Surrey, UK; 20μl per 10^7 $CD4^+$ cells). For selection of the $CD4^+CD25^+$ component, positive cells were isolated by magnetic separation using the MACS system (Miltenyi Biotec Ltd., Woking, Surrey, UK), while the $CD4^+CD25^{neg}$ effector cells were obtained from the negative fraction in the cell separation column. On re-analysis, $CD4^+CD25^+$ cells expressed Foxp3 to a purity of over 85%.

Bone marrow transplantation

Bone marrow was harvested from 8-12 week-old shPhd2#9 or control (Ctrl) donors (both CD45.2, C57BL/6 background) by flushing tibias and femurs with PBS (Gibco BRL, Thermo Fisher, Waltham, Massachusetts) supplemented with 2% bovine serum albumin (BSA, Sigma-Aldrich, Poole, Dorset, UK). Single cell suspensions, minus settled aggregates, were washed once with PBS/BSA through a 70μm-nylon cell strainer (Falcon, Corning, New York). Treated recipient mice (CD45.1, C57BL/6,) received a split lethal dose of 4.5+4.5 Gy total body irradiation (TBI) followed by injection of $5x10^6$ bone marrow cells intravenously. Antibiotic prophylaxis with co-trimoxazole in drinking water was provided to mice before and immediately after transplantation. Mice were monitored by serial flow cytometric analysis of the peripheral blood. Eight weeks after irradiation and transplantation, cohorts of mice were started on doxycycline treatment as indicated.

Skin transplantation

CBA (CBA, H-2^k), C57BL/6 (B6, H-2^b), and C57BL/6 Rag $1^{-/-}$ (H-2^b) mice were obtained from and housed in the Biomedical Services Unit of the John Radcliffe Hospital (Oxford, UK) in individually ventilated cages, with the only reported positives on health screening over the entire time course of these studies being for *Helicobacter spp*, occasional mouse norovirus and *Tritrichomonas spp*. Food and water was provided *ad libitum* and animals were maintained on a 12 hour light/dark cycle. Mice were randomized and groups split across cages. All scoring was blinded and no animals were excluded from the study. Sex-matched mice between 6-12 weeks of age at the time of first experimental procedure were used in all experiments. T cell-deficient (C57BL/6 Rag$1^{-/-}$) mice were reconstituted intravenously with 1x10^4 $CD4^+25^{neg}$ effector cells from C57BL/6 mice with or without 1-5x10^4 $CD4^+CD25^+$ cells from WT C57BL/6, shPhd2#9 or control (Ctrl) animals. The day after reconstitution, mice received a CBA skin graft under general anaesthetic. Full-thickness tail skin was transplanted to graft beds on the flanks of recipient mice (67). Grafts were then monitored daily, and graft rejection was defined by complete destruction of the skin.

In vitro suppression assays

Sample processing, cell isolation, and *in vitro* T cell analyses were performed in the Transplantation Research Immunology Group following established laboratory protocols. Assay performance and data reporting conforms with the *Minimal Information About T cell Assays* (MIATA) guidelines (68) and the *Minimum Information about Tregs* (MITREG) guidelines (69). For *in vitro* suppression assays, splenocytes from shPhd2#9 or control (Ctrl) C57BL/6 (H-2^b) mice pre-treated with doxycycline water for four weeks were used as a source of $CD4^+CD25^+$ cells. $CD4^+CD25^+$ cells and effector T cells (Teffs, $CD4^+CD25^{neg}$) were isolated using a Dynabeads Untouched Mouse CD4 Cells kit (Invitrogen, Thermo Fisher, Waltham, Massachusetts, cat 11415D) followed by $CD25^+$ cell enrichment using an anti-CD25-PE antibody (eBioscience, Thermo Fisher, Waltham, Massachusetts, clone PC61.5) and anti-PE Microbeads (Miltenyi Biotec Ltd., Woking, Surrey, UK, cat 130-048-801). Cells were counted using trypan blue staining, a hemocytometer, and microscope. Cells were cultured at 37°C and 5% CO_2 in complete medium consisting of RPMI-1640 (Sigma Aldrich, Poole,

Dorset, UK) supplemented with 10% FBS, penicillin/streptomycin (Sigma Aldrich, Poole, Dorset, UK) and L-glutamine (Sigma Aldrich, Poole, Dorset, UK). Wild-type C57BL/6 or control Teffs at $1x10^5$/well were stimulated with $1x10^5$/well of anti-CD3/anti-CD28 Dynabeads (Invitrogen, Thermo Fisher, Waltham, Massachusetts, cat: 11456D). Syngeneic Tregs were added at 1:1, 1:2 ratios (Treg:Teff) and further serial dilutions. Doxycycline at 1μg/ml was added to all wells and replenished every day. Cells were incubated for 5 days and ^{3}H thymidine (Perkin Elmer, Beaconsfield, Buckinghamshire, UK) added for the final 18 hours of culture. For suppression assays using allogeneic dendritic cells (DCs) as stimulators, $2x10^4$ previously cryopreserved CBA (H-2^k) DCs were added per well instead of beads. Data were obtained as count per minute (cpm) using a Betaplate reader and recalculated as division index. CBA DCs were generated from bone marrow cultured for six days in complete RPMI with GM-CSF and IL-4 (both Peprotech, Rocky Hill, New Jersey) with cytokines being replaced every second day. DCs were then cryopreserved in medium containing 45% FBS, 45% RPMI and 10% DMSO (Sigma Aldrich, Poole, Dorset, UK) and stored in vapour phase liquid nitrogen until required.

TSDR analysis

Methylation at the Treg-specific demethylated region (TSDR) was assessed in flow-sorted CD4+Foxp3+ and CD4+Foxp3- cells from doxycycline-treated shPhd2#9 or control mice. Methylation analysis was conducted by EpigenDx (Hopkinton, Massachusetts) by pyrosequencing of bisulphite-modified DNA purified from frozen cells. 4 representative CpG residues of the mouse *Foxp3* TSDR were analysed using assay ADS568-FS2. The demethylation percentage on the active X chromosome was calculated; data from female mice were adjusted to allow for complete methylation of the TSDR on the inactivated X chromosome.

Statistical analyses

The statistical tests used are stated in each figure legend. All statistical analyses were conducted using GraphPad Prism software (GraphPad Software Inc., La Jolla, California). A one-way ANOVA was used for multi-group comparisons together with Tukey's or Dunnett's multiple comparisons *post hoc* tests. Groups

with two independent variables were tested using a two-way ANOVA with Šídák's correction for multiple comparisons. A repeated measures ANOVA was used to compare groups over time. Unpaired 2-tailed Student's *t* tests were used to assess two independent groups. Allograft survival data were analyzed using the log-rank test. *p* values <0.05 were taken as statistically significant.

Study approval

All mouse experiments were performed using protocols approved by the Committee on Animal Care and Ethical Review at the University of Oxford and in accordance with the UK Animals (Scientific Procedures) Act 1986 and under PPL numbers 30-3050, 30-2966, P38BE32DE and P8869535A.

AUTHOR CONTRIBUTIONS

Experiments were designed by CWP, AY, FI, JH and PJR.

LD provided reagents and expertise relating to the development of the knockdown mice. MLC and AY designed and tested the shRNA sequences; AY, BD and DB created the knockdown mice, with input from CWP and PJR.

TB and XC supplied and genotyped the knockout animals with input from CWP and PJR.

KB, TC and EC undertook the anti-nuclear antibody assays in a blinded fashion on samples provided by AY and PSM.

CLS, PSM, RG, LS and HK contributed to the histopathological analyses.

KKr and HL performed parallel experiments in a separate animal facility that corroborated findings reported in this paper.

AY, FI, JH, JM, MU, KM and KKa acquired and analysed the flow cytometry data.

Data were predominantly analyzed and interpreted by AY, FI, JH, CWP and PJR with contributions from the other authors. AY and FI performed statistical analyses.

The manuscript was written by CWP, PJR and FI with input from AY, JH, PSM, BD, CLS and then reviewed by all the authors. Figures were prepared by AY, PSM and KKa with input from the rest of the writing group.

ACKNOWLEDGEMENTS

We thank Scott Lowe for providing access to the KH2 embryonic stem cells, expertise and associated constructs for generation of the doxycycline-inducible knockdown mice and the Genome Engineering Core at the Wellcome Trust Centre for Human Genetics (funded by Wellcome Trust grant reference 203141/Z/16/Z) for the generation of the mouse models. Daniel Royston, Ian Roberts and Gordon Stamp all contributed helpful opinions on the histopathology. We thank Georg Hollander, Annina Graedel and Thomas Riffelmacher for undertaking exploratory experiments relating to the role of the thymus and T cell subsets that in the end did not form part of this manuscript. We also thank Chris O'Callaghan, Lucy Davison, Richard Cornall, Katja Simon, Moira Whyte, Sarah Walmsley and all members of the Oxygen-sensing group in Oxford, but particularly David Mole, Julie Adam and Norma Masson, for helpful discussions relating to the overall phenotype.

We thank Douglas Dos Santos Passos, Viv Clark, Roo Bhasin, Jordan Tanner and all the staff of the Functional Genetics Facility of the Wellcome Trust Centre for Human Genetics and the Biomedical Services Unit of the John Radcliffe Hospital, University of Oxford, UK for their care of the animals used in this work.

We are grateful to the Wellcome Trust (106241/Z/14/Z), Kidney Research UK (SF1/2014), EU FP7 project BIO-DrIM (305147) and the Oxford Branch of the Ludwig Institute for Cancer Research for financial support of this work. PSM is supported by a Jean Shanks Foundation/Pathological Society of Great Britain and Ireland Research Training Fellowship. FI held a NIHR Clinical Lectureship (CL-2013-13-005) and is now a Wellcome Trust CRCD Fellow (211122/Z/18/Z). This work was also supported by the Francis Crick Institute which receives its core funding from Cancer Research UK (FC001501), the UK Medical Research Council (FC001501), and the Wellcome Trust (FC001501).

REFERENCES

1. Kaelin WG, Jr., Ratcliffe PJ. Oxygen sensing by metazoans: the central role of the HIF hydroxylase pathway. *Mol Cell.* 2008;30(4):393-402.
2. Schofield CJ, Ratcliffe PJ. Oxygen sensing by HIF hydroxylases. *Nat Rev Mol Cell Biol.* 2004;5(5):343-354.
3. Semenza GL. HIF-1 mediates metabolic responses to intratumoral hypoxia and oncogenic mutations. *J Clin Invest.* 2013;123(9):3664-3671.
4. Semenza GL. Surviving ischemia: adaptive responses mediated by hypoxia-inducible factor 1. *J Clin Invest.* 2000;106(7):809-812.
5. Pugh CW, Ratcliffe PJ. New horizons in hypoxia signaling pathways. *Exp Cell Res.* 2017;356(2):116-121.
6. Palazon A, Goldrath AW, Nizet V, Johnson RS. HIF transcription factors, inflammation, and immunity. *Immunity.* 2014;41(4):518-528.
7. Kominsky DJ, Campbell EL, Colgan SP. Metabolic shifts in immunity and inflammation. *J Immunol.* 2010;184(8):4062-4068.
8. Manresa MC, Taylor CT. Hypoxia Inducible Factor (HIF) Hydroxylases as Regulators of Intestinal Epithelial Barrier Function. *Cell Mol Gastroenterol Hepatol.* 2017;3(3):303-315.
9. Keeley TP, Mann GE. Defining Physiological Normoxia for Improved Translation of Cell Physiology to Animal Models and Humans. *Physiological Reviews.* 2019;99(1):161-234.
10. Airley RE, Monaghan JE, Stratford IJ. Hypoxia and disease: opportunities for novel diagnostic and therapeutic prodrug strategies. *The Pharmaceutical Journal.* 2000;264(7094):666-673.
11. Haase VH. HIF-prolyl hydroxylases as therapeutic targets in erythropoiesis and iron metabolism. *Hemodial Int.* 2017;21 Suppl 1:S110-S124.
12. Takeda K, Cowan A, Fong GH. Essential role for prolyl hydroxylase domain protein 2 in oxygen homeostasis of the adult vascular system. *Circulation.* 2007;116(7):774-781.
13. Takeda K, Ho VC, Takeda H, Duan LJ, Nagy A, Fong GH. Placental but not heart defects are associated with elevated hypoxia-inducible factor alpha levels in mice lacking prolyl hydroxylase domain protein 2. *Mol Cell Biol.* 2006;26(22):8336-8346.
14. Takeda K, et al. Regulation of adult erythropoiesis by prolyl hydroxylase domain proteins. *Blood.* 2008;111(6):3229-3235.
15. Minamishima YA, Moslehi J, Bardeesy N, Cullen D, Bronson RT, Kaelin WG, Jr. Somatic inactivation of the PHD2 prolyl hydroxylase causes polycythemia and congestive heart failure. *Blood.* 2008;111(6):3236-3244.
16. Caldwell CC, et al. Differential effects of physiologically relevant hypoxic conditions on T lymphocyte development and effector functions. *J Immunol.* 2001;167(11):6140-6149.
17. Lukashev D, et al. Cutting edge: hypoxia-inducible factor 1alpha and its activation-inducible short isoform I.1 negatively regulate functions of CD4+ and CD8+ T lymphocytes. *J Immunol.* 2006;177(8):4962-4965.
18. Ben-Shoshan J, Maysel-Auslender S, Mor A, Keren G, George J. Hypoxia controls CD4+CD25+ regulatory T-cell homeostasis via hypoxia-inducible factor-1alpha. *Eur J Immunol.* 2008;38(9):2412-2418.
19. Shi LZ, et al. HIF1alpha-dependent glycolytic pathway orchestrates a metabolic checkpoint for the differentiation of TH17 and Treg cells. *J Exp Med.* 2011;208(7):1367-1376.
20. Dang EV, et al. Control of T(H)17/T(reg) balance by hypoxia-inducible factor 1. *Cell.* 2011;146(5):772-784.
21. Kryczek I, et al. Human TH17 cells are long-lived effector memory cells. *Sci Transl Med.* 2011;3(104):104ra100.
22. Clambey ET, et al. Hypoxia-inducible factor-1 alpha-dependent induction of FoxP3 drives regulatory T-cell abundance and function during inflammatory hypoxia of the mucosa. *Proc Natl Acad Sci U S A.* 2012;109(41):E2784-2793.
23. Finlay DK, et al. PDK1 regulation of mTOR and hypoxia-inducible factor 1 integrate metabolism and migration of CD8+ T cells. *J Exp Med.* 2012;209(13):2441-2453.

24. McNamee EN, Korns Johnson D, Homann D, Clambey ET. Hypoxia and hypoxia-inducible factors as regulators of T cell development, differentiation, and function. *Immunol Res.* 2013;55(1-3):58-70.
25. Doedens AL, et al. Hypoxia-inducible factors enhance the effector responses of CD8(+) T cells to persistent antigen. *Nat Immunol.* 2013;14(11):1173-1182.
26. Gomez-Rodriguez J, et al. Itk-mediated integration of T cell receptor and cytokine signaling regulates the balance between Th17 and regulatory T cells. *J Exp Med.* 2014;211(3):529-543.
27. Wang H, Flach H, Onizawa M, Wei L, McManus MT, Weiss A. Negative regulation of Hif1a expression and TH17 differentiation by the hypoxia-regulated microRNA miR-210. *Nat Immunol.* 2014;15(4):393-401.
28. Hsiao HW, et al. Deltex1 antagonizes HIF-1alpha and sustains the stability of regulatory T cells in vivo. *Nat Commun.* 2015;6:6353.
29. Lee JH, Elly C, Park Y, Liu YC. E3 Ubiquitin Ligase VHL Regulates Hypoxia-Inducible Factor-1alpha to Maintain Regulatory T Cell Stability and Suppressive Capacity. *Immunity.* 2015;42(6):1062-1074.
30. Tao JH, Barbi J, Pan F. Hypoxia-inducible factors in T lymphocyte differentiation and function. A Review in the Theme: Cellular Responses to Hypoxia. *Am J Physiol Cell Physiol.* 2015;309(9):C580-589.
31. Xu Y, et al. Glycolysis determines dichotomous regulation of T cell subsets in hypoxia. *J Clin Invest.* 2016;126(7):2678-2688.
32. Thompson AA, et al. Hypoxia determines survival outcomes of bacterial infection through HIF-1alpha dependent re-programming of leukocyte metabolism. *Sci Immunol.* 2017;2(8).
33. Overacre-Delgoffe AE, et al. Interferon-gamma Drives Treg Fragility to Promote Anti-tumor Immunity. *Cell.* 2017;169(6):1130-1141.
34. Sadiku P, et al. Prolyl hydroxylase 2 inactivation enhances glycogen storage and promotes excessive neutrophilic responses. *J Clin Invest.* 2017;127(9):3407-3420.
35. Dow LE, et al. A pipeline for the generation of shRNA transgenic mice. *Nat Protoc.* 2012;7(2):374-393.
36. Kingsley CI, Nadig SN, Wood KJ. Transplantation tolerance: lessons from experimental rodent models. *Transpl Int.* 2007;20:828-841.
37. Nasr Z, et al. Suppression of eukaryotic initiation factor 4E prevents chemotherapy-induced alopecia. *BMC Pharmacol Toxicol.* 2013;14:58.
38. Miething C, et al. PTEN action in leukaemia dictated by the tissue microenvironment. *Nature.* 2014;510(7505):402-406.
39. Bolden JE, et al. Inducible in vivo silencing of Brd4 identifies potential toxicities of sustained BET protein inhibition. *Cell Rep.* 2014;8(6):1919-1929.
40. Ebbesen SH, et al. Pten loss promotes MAPK pathway dependency in HER2/neu breast carcinomas. *Proc Natl Acad Sci U S A.* 2016;113(11):3030-3035.
41. Brunkow ME, et al. Disruption of a new forkhead/winged-helix protein, scurfin, results in the fatal lymphoproliferative disorder of the scurfy mouse. *Nat Genet.* 2001;27(1):68-73.
42. Bennett CL, et al. The immune dysregulation, polyendocrinopathy, enteropathy, X-linked syndrome (IPEX) is caused by mutations of FOXP3. *Nat Genet.* 2001;27(1):20-21.
43. Chatila TA, et al. JM2, encoding a fork head-related protein, is mutated in X-linked autoimmunity-allergic disregulation syndrome. *J Clin Invest.* 2000;106(12):R75-81.
44. Polansky JK, et al. DNA methylation controls Foxp3 gene expression. *Eur J Immunol.* 2008;38:1654-1663.
45. Sawant DV, Vignali DA. Once a Treg, always a Treg? *Immunol Rev.* 2014;259(1):173-191.
46. Hori S. Lineage stability and phenotypic plasticity of Foxp3(+) regulatory T cells. *Immunol Rev.* 2014;259(1):159-172.
47. Sugimoto N, et al. Foxp3-dependent and -independent molecules specific for CD25+CD4+ natural regulatory T cells revealed by DNA microarray analysis. *Int Immunol.* 2006;18(8):1197-1209.
48. Hill JA, et al. Foxp3 transcription-factor-dependent and -independent regulation of the regulatory T cell transcriptional signature. *Immunity.* 2007;27(5):786-800.
49. Delgoffe GM, et al. Stability and function of regulatory T cells is maintained by a neuropilin-1-semaphorin-4a axis. *Nature.* 2013;501(7466):252-256.

50. Ouyang W, et al. Novel Foxo1-dependent transcriptional programs control T(reg) cell function. *Nature.* 2012;491(7425):554-559.
51. Pan F, et al. Eos mediates Foxp3-dependent gene silencing in CD4+ regulatory T cells. *Science.* 2009;325(5944):1142-1146.
52. Mellor AL, Munn DH. Physiologic control of the functional status of Foxp3+ regulatory T cells. *J Immunol.* 2011;186(8):4535-4540.
53. Lund JM, Hsing L, Pham TT, Rudensky AY. Coordination of early protective immunity to viral infection by regulatory T cells. *Science.* 2008;320(5880):1220-1224.
54. Sharma MD, et al. Reprogrammed foxp3(+) regulatory T cells provide essential help to support cross-presentation and CD8(+) T cell priming in naive mice. *Immunity.* 2010;33(6):942-954.
55. O'Gorman WE, et al. The initial phase of an immune response functions to activate regulatory T cells. *J Immunol.* 2009;183(1):332-339.
56. Wan S, Xia C, Morel L. IL-6 produced by dendritic cells from lupus-prone mice inhibits CD4+CD25+ T cell regulatory functions. *J Immunol.* 2007;178(1):271-279.
57. Pasare C, Medzhitov R. Toll pathway-dependent blockade of CD4+CD25+ T cell-mediated suppression by dendritic cells. *Science.* 2003;299(5609):1033-1036.
58. Li L, Kim J, Boussiotis VA. IL-1beta-mediated signals preferentially drive conversion of regulatory T cells but not conventional T cells into IL-17-producing cells. *J Immunol.* 2010;185(7):4148-4153.
59. Coyne DW, Goldsmith D, Macdougall IC. New options for the anemia of chronic kidney disease. *Kidney International Supplements.* 2017;7:157-163.
60. Knowles HJ, Tian YM, Mole DR, Harris AL. Novel mechanism of action for hydralazine: induction of hypoxia-inducible factor-1alpha, vascular endothelial growth factor, and angiogenesis by inhibition of prolyl hydroxylases. *Circ Res.* 2004;95(2):162-169.
61. Cameron HA, Ramsay LE. The lupus syndrome induced by hydralazine: a common complication with low dose treatment. *Br Med J (Clin Res Ed).* 1984;289(6442):410-412.
62. Courtney KD, et al. Phase I Dose-Escalation Trial of PT2385, a First-in-Class Hypoxia-Inducible Factor-2alpha Antagonist in Patients With Previously Treated Advanced Clear Cell Renal Cell Carcinoma. *J Clin Oncol.* 2018;36(9):867-874.
63. Premsrirut PK, Dow LE, Park Y, Hannon GJ, Lowe SW. Creating transgenic shRNA mice by recombinase-mediated cassette exchange. *Cold Spring Harb Protoc.* 2013;2013(9):835-842.
64. Hodson EJ, et al. Regulation of ventilatory sensitivity and carotid body proliferation in hypoxia by the PHD2/HIF-2 pathway. *J Physiol.* 2016;594(5):1179-1195.
65. Silver KL, Crockford TL, Bouriez-Jones T, Milling S, Lambe T, Cornall RJ. MyD88-dependent autoimmune disease in Lyn-deficient mice. *Eur J Immunol.* 2007;37(10):2734-2743.
66. Appelhoff RJ, et al. Differential function of the prolyl hydroxylases PHD1, PHD2, and PHD3 in the regulation of hypoxia-inducible factor. *J Biol Chem.* 2004;279(37):38458-38465.
67. Kingsley CI, Karim M, Bushell AR, Wood KJ. CD25+CD4+ regulatory T cells prevent graft rejection: CTLA-4 and IL-10 dependent immunoregulation of alloresponses. *J Immunol.* 2002;168:1080-1086.
68. Janetzki S, et al. "MIATA"-minimal information about T cell assays. *Immunity.* 2009;31(4):527-528.
69. Fuchs A, et al. Minimum Information about T Regulatory Cells: A Step toward Reproducibility and Standardization. *Front Immunol.* 2017;8:1844.

Figure 1. shPhd2#9 mice develop leukocyte expansion on doxycycline treatment. (**A**) Representative image of a shPhd2#9 mouse and its littermate control (Ctrl) treated with doxycycline (2mg/mL with 30% sucrose drinking-water *ad libitum*) for 4-5 weeks. (**B**) Representative brightfield and GFP images of peripheral lymph nodes (pLN) from a shPhd2#9 mouse and its littermate control (Ctrl). Scale bar: 1cm (**C**) Wet weight of pLNs (x4) and spleens (x1) from shPhd2#9 mice (n=6) and their littermate control (Ctrl, n=6). Unpaired, independent groups of 2 were analyzed using a 2-tailed Student's *t* test. Data are represented as means ± SEM. H&E staining of tissues from shPhd2#9 and littermate control (Ctrl) mice: pLN (x2.5 (**D**-**E**), x10 (**F**) and x80 (**G**)), arrows indicate cells with oval, vesicular nuclei and eosinophilic cytoplasm; spleen (x5 (**H**-**I**)); skin (x20 (**J**-**K**) and x80 (**L**)), arrows demonstrate exocytosis of lymphocytes into the epidermis; lung (x10 (**M**)); kidney (x20 (**N**) and x40 (**O**-**P**)); liver (x40 (**Q**)); heart (x40 (**R**)), arrow indicates a focal collection of mononuclear inflammatory cells at the epicardial surface of the heart. The scale bar is 500μm at x2.5 and proportionately smaller lengths at higher magnifications. Each symbol in (**C**) represents an individual mouse. Data are representative of those obtained in three independent experiments at this time point.

***p<0.001; ****p<0.0001.

Figure 2. Reduction of *Hif2a* expression reverses the phenotype in inducible *Phd2* knockdown and *Phd2* knockout mice. (**A**) FACS analysis of cells in peripheral lymph nodes (pLNs) from shPhd2#9 (*Phd2* knockdown), shPhd2Hif1 (*Phd2* knockdown/*Hif1a* knockdown), shPhd2Hif2 (*Phd2* knockdown/*Hif2a* knockdown) and control (Ctrl) mice for CD45, CD3, B220, and Gr1 expression. Mice were treated with doxycycline (2mg/mL with 30% sucrose drinking-water *ad libitum*) for 4 weeks. Data from individual mice and means ± SEM are represented. Groups were compared using a one-way ANOVA with Tukey's post hoc tests. (**B**) Representative brightfield images and wet weight of peripheral lymph nodes (pLN) from the same mice. Data are represented as means ± SEM. Scale bar: 1cm. (**C**) Mean body weight changes (% relative to day 0) of the same mice during doxycycline treatment. Data are represented as means ± SD, with at least n=3 per group. Groups were compared by a repeated measures ANOVA with Tukey's multiple comparisons post hoc test: Ctrl vs shPhd2#9 (***); Ctrl vs shPhd2Hif1 (**); Ctrl vs shPhd2Hif2 (ns); shPhd2#9 vs shPhd2Hif1 (ns); shPhd2#9 vs shPhd2Hif2 (***); shPhd2Hif2 vs shPhd2Hif1 (***). (**D**) FACS analysis for CD45, CD3, B220, and Gr1 expression

by cells in pLNs from conditional Phd2ko (*Phd2* knockout), Phd2Hif1ko (*Phd2* knockout/*Hif1a* knockout), Phd2Hif2ko (*Phd2* knockout/*Hif2a* knockout) and control (Ctrl) mice 4 weeks after tamoxifen treatment. Data from individual mice and means ± SEM are represented. Groups were compared using a one-way ANOVA with Tukey's post hoc tests. (**E**) Representative brightfield images and wet weight of pLNs from the same mice. Data are represented as means ± SEM. Scale bar: 1cm. Multigroup comparisons were analyzed by a one-way ANOVA with Tukey's multiple comparisons post hoc test. Each symbol in (**A**)-(**E**) represents an individual mouse. Data were consistent over three independent experiments.

**p*<0.05; ***p*<0.01; ****p*<0.001; ns=not significant.

Figure 3. Concomitant *Hif2a* silencing ablates tissue inflammation in *Phd2* knockdown mice. H&E staining of skin (x20), kidney (x10) and liver (x10, arrows demonstrate periportal and perivenous mononuclear inflammatory cell infiltrates) from shPhd2#9 (*Phd2* knockdown), shPhd2Hif1 (*Phd2* knockdown/*Hif1a* knockdown), shPhd2Hif2 (*Phd2* knockdown/*Hif2a* knockdown) and control (Ctrl) mice treated for 4 weeks with doxycycline. The scale bar is 125μm at x10 and proportionately smaller lengths at higher magnifications. Each column of images is representative of multiple sections from each organ from the same mouse. In this experiment tissues form two mice of each genotype were examined.

Figure 4. Phenotype reversal following withdrawal of doxycycline. (**A**) Representative brightfield images and wet weight of peripheral lymph nodes (pLNs) from shPhd2#9 mice and their littermate controls (Ctrl) maintained on doxycycline for 3-4 weeks (Dox-ON group) or treated with doxycycline for 3-4 weeks and then analyzed 7 weeks after doxycycline withdrawal (Dox-ON/OFF group). Scale bars: 1cm. Data are represented as means ± SEM with n=4 per group. Multi-group comparisons were analyzed by one-way ANOVA with Tukey's multiple comparisons post hoc test. (**B**) Mean body weight changes (%) of shPhd2#9 and Ctrl mice, relative to day 0 of doxycycline treatment or doxycycline withdrawal. Data are represented as means ± SD, with n=7-8 per group. Groups were compared using a two-way ANOVA. (**C**) Representative fluorescent image of anti-nuclear antibodies (ANA) using mouse serum from Dox-ON and Dox-ON/OFF groups of shPhd2#9 and Ctrl mice. Scale bars: 50μm. H&E staining of skin (x20 (**D**-**E**)), kidney (x2.5 (**F**-**G**); x10 (**H**-**I**)) and lung (x10 (**J**-**K**))

from Dox-ON and Dox-ON/OFF groups of shPhd2#9 mice. The scale bar is 500 μm at x2.5 and proportionately smaller lengths at higher magnifications. (**L**) FACS analysis of cells from pLNs from Dox-ON and Dox-ON/OFF groups of shPhd2#9 and Ctrl mice, analyzed for CD45, CD3, B220 and Gr1 expression. Data are represented as means ± SEM with at least n=4 per group. Unpaired, independent groups of 2 were analyzed using a 2-tailed Student's *t* test. Each symbol in (**A**) and (**L**) represents an individual mouse. Data were consistent over two independent experiments.

**p*<0.05; ****p*<0.001; *****p*<0.0001; ns=not significant.

Figure 5. Transfer of the *Phd2* knockdown phenotype by bone marrow transplantation (BMT). (**A**) Representative brightfield images and tissue weights of peripheral lymph nodes (pLN) from BMT recipients following 10 weeks treatment with doxycycline (2mg/mL with 30% sucrose drinking-water *ad libitum*). Syngeneic congenically marked (CD45.1) mice were lethally-irradiated before receiving CD45.2 shPhd2#9 bone marrow (BMT-shPhd2#9, n=6) or CD45.2 control bone marrow (BMT-Ctrl, n=2) and allowed to reconstitute for 8 weeks prior to doxycycline treatment. Scale bars: 1cm. Data are represented as means ± SEM. (**B**) FACS analysis of cells in pLNs from BMT-Ctrl and BMT-shPhd2#9 mice, analyzed for $CD45.2^+$, $CD45.2^+CD3^+$, $CD45.2^+CD19^+$, and $CD45.2^+Gr1^+$ expression. Data are represented as means ± SEM. (**C**) Representative fluorescent image of anti-nuclear antibodies (ANAs) using mouse serum from BMT recipients. Scale bars: 50μm. H&E staining of the pLN (x2.5 (**D**-**E**)) and liver (x5 (**F**-**G**)) from BMT recipient mice. Arrows indicate inflammatory foci. The scale bar is 500μm at x2.5 and proportionately smaller lengths at higher magnifications. Each symbol in (**A**) and (**B**) represents an individual mouse. The same experiment was repeated twice independently.

Figure 6. Enumeration and TSDR analysis of cells bearing helper, effector and regulatory markers in *Phd2* knockdown and knockout mice. (**A**) Gating strategy and enumeration of single positive ($CD4^+CD8^-$ or $CD4^-CD8^+$), double positive ($CD4^+CD8^+$) and double negative ($CD8^-CD4^-$) cells within lymph nodes (pLNs) of control (Ctrl) and shPhd2#9 mice following 4 weeks of doxycycline treatment (2mg/mL with 30% sucrose drinking-water *ad libitum*). (**B**) Expression of Foxp3 and CD25 within $CD4^+$ populations within lymph nodes (pLNs) of

control (Ctrl) and shPhd2#9 mice following 4 weeks of doxycycline treatment. (**C**) $CD45.2^+CD3^+CD4^+Foxp3^+$ cell numbers in pLNs from lethally-irradiated syngeneic $CD45.1^+$ congenically marked mice receiving bone marrow transplants (BMT) from $CD45.2^+$ shPhd2#9 or $CD45.2^+$ Ctrl mice. (**D**) $CD3^+CD4^+Foxp3^+$ cell numbers in the peripheral lymph nodes (pLNs) of shPhd2#9 mice and their littermate controls (Ctrl), treated with doxycycline for 3-4 weeks and analyzed directly (ON) or 7 weeks after doxycycline withdrawal (ON/OFF) (n=7-8, two independent assays). (**E**) $CD3^+CD4^+Foxp3^+$ cell numbers in pLNs from shPhd2#9 (*Phd2* knockdown), shPhd2Hif1 (*Phd2* knockdown/*Hif1a* knockdown), shPhd2Hif2 (*Phd2* knockdown/*Hif2a* knockdown) and Ctrl mice. (**F**) $CD3^+CD4^+Foxp3^+$ cell numbers in pLNs from Phd2ko (*Phd2* knockout), Phd2Hif1ko (*Phd2* knockout/*Hif1a* knockout), Phd2Hif2ko (*Phd2* knockout/*Hif2a* knockout) and Ctrl mice. (**G**) Flow sorted $CD4^+Foxp3^+$ or $CD4^+Foxp3^-$ cells from Ctrl or shPhd2#9 mice that were treated for 4 weeks with doxycycline were analyzed for the percentage demethylation of their TSDR on the active X chromosome by pyrosequencing. Data are represented as means ± SEM with at least n=3 per group. Unpaired, independent groups of 2 were analyzed using a 2-tailed Student's *t* test. Multigroup comparisons were analyzed by one-way ANOVA with Tukey's or Dunnett's multiple comparisons post hoc test. TSDR data were analyzed by two-way ANOVA with Šídák's correction for multiple comparisons. Each symbol represents an individual mouse. Data in panels (**C**)-(**G**) are representative of two independent experiments.

**p*<0.05; ***p*<0.01; ****p*<0.001.

Figure 7. Treg functional assays. (**A**) Schematic of *in vivo* experimental plan. C57BL/6 $Rag1^{-/-}$ ($H\text{-}2^b$) mice received $CD4^+CD25^{neg}$ effector T cells (Teff) with or without $H2^b$ $CD4^+CD25^+$ cells from shPhd2#9 or control (Ctrl) mice that had either received 1 week doxycycline (2mg/ml in drinking water, *ad libitum*) pre-treatment or no doxycycline pre-treatment. One day later, mice received an allogeneic $H\text{-}2^k$ skin graft. Mice receiving cells from doxycycline treated donors remained on doxycycline (**B**) whereas those receiving cells from untreated donors started doxycycline treatment from day 2 after transplantation (**C**). Allograft survival was monitored until rejection. (**B**) Survival graph with adoptively transferred cells derived from 1 week doxycycline pre-treated mice. (**C**) Survival graph with adoptively-transferred cells derived from mice only treated with doxycycline after adoptive transfer. Survival data were analyzed using the log-rank test for both

(B) and (C). The number of animals in each group is indicated. (**D**) Schematic of *in vitro* experimental plan. $1x10^5$/well control C57BL/6 WT Teffs ($CD4^+CD25^-$ responders, R) were stimulated (S) with $1x10^5$/well anti-CD3/anti-CD28 beads or $2x10^4$ CBA ($H\text{-}2^k$) dendritic cells (DCs). $CD4^+CD25^+$ cells from shPhd2#9 or Ctrl mice were added at 1:1, 1:2, 1:4 and 1:8 ratios relative to Teff responders. Doxycycline at 1μg/mL was added to all wells and replenished daily. Cells were incubated for 5 days and ^{3}H-thymidine added for the final 18 hours of culture. Proliferation levels were normalized to positive control (R+S). (**E**) *In vitro* suppression assay using anti-CD3/anti-CD28 as stimulators. (**F**) *In vitro* suppression assay using DCs as stimulators. Data are represented as means ± SEM of biological replicates. Unpaired, independent groups (1:1, 1:2, 1:4, and 1:8) of 2 were analyzed using 2-tailed Student's *t* tests in (**E**) and (**F**).

**p*<0.05; ***p*<0.01; *****p*<0.0001; ns=not significant.

Figure 8. *Phd2* knockdown $CD4^+CD25^+$ cells alone can induce skin allograft rejection. (**A**) Schematic of *in vivo* experimental plan. C57BL/6 $Rag1^{-/-}$ ($H\text{-}2^b$) mice received <u>either:</u> $5x10^4$ $H2^b$ $CD4^+CD25^+$ cells from shPhd2#9 mice; $5x10^4$ $H2^b$ $CD4^+CD25^+$ cells from control (Ctrl) mice; or $5x10^4$ $H2^b$ wild type $CD4^+CD25^-$ effector cells alone. One day later, mice received an allogeneic $H\text{-}2^k$ skin graft, followed by doxycycline treatment (2mg/ml in drinking water, *ad libitum*) from day 2 post-transplantation. Allograft survival was monitored until rejection. The number of animals in each group is indicated. (**B**) Skin allograft survival graph. Survival data were analyzed using the log-rank test. The censored data point in the shPhd2#9 group represents a mouse that developed weight loss and a generalized inflammatory phenotype.

***p*<0.01

Figure 9. Expression patterns of T cell related cytokines and transcription factors in shPhd2#9 mice. (**A**) Representative flow cytometry plots demonstrating expression of T-bet, TNF-α, IFN-γ, IL-4, GATA-3, IL-17, ROR-γt, IL-2 and IL-10 against Foxp3 within the total $CD4^+$ populations from lymph nodes (pLNs) of control (Ctrl, left) and shPhd2#9 mice (right) following 4 weeks of doxycycline treatment (2mg/ml with 30% sucrose drinking-water *ad libitum*). (**B**) Percentage of cells expressing T-bet, TNF-α, IFN-γ, IL-4, GATA-3, IL-17, ROR-γt, IL-2 and IL-10 within $CD4^+$ $Foxp3^-$ (left) or $CD4^+$ $FoxP3^+$ cell populations (right) from pLNs of Ctrl and shPhd2#9

mice after 4 weeks of doxycycline treatment (n = 6 mice per group). Data are represented as means ± SEM, analyzed using 2-tailed Student's *t* tests.

*p<0.05; **p<0.01; ***p<0.001; ****p<0.0001; ns=not significant

Figure 10. Identification of naïve and memory T cells in shPhd2#9 mice. Dot plots and quantification of naïve (T_N, $CD44^{lo}CD62L^{hi}$), central memory (T_{CM}, $CD44^{hi}CD62L^{hi}$) and effector memory (T_{EM}, $CD44^{hi}CD62L^{lo}$) T cells within pLNs of control (Ctrl, left) and shPhd2#9 mice (right) following 4 weeks of doxycycline treatment (2mg/ml with 30% sucrose drinking-water *ad libitum*) (n = 6 mice per group). Data are represented as means ± SEM, analyzed using 2-tailed Student's *t*-tests.

**p<0.01; ***p<0.001; ****p<0.0001; ns=not significant.

Supplementary Table 1. shRNA sequences and validation of target gene knockdown. Sequences were introduced by lentiviral infection into mouse embryonic fibroblasts (MEF) and recombinase-mediated cassette exchange (RCME) into KH2 ES cells. Following 48 hours of doxycycline treatment (2μg/mL) target gene mRNA levels were measured, normalized against *Beta-Actin* and % knockdown in transgenic cells was compared with control cells which received shRNA against *Firefly-Luciferase*. Induction of HIF target gene mRNA included *Phd3* (x3.5 and x 4.9 fold) and *Bnip3* (x5.2 and x5.1 fold) by *Phd2#3* and *Phd2#9* sequences respectively. Data are represented as means from n=3.

Supplementary Figure 1. Inducible shRNA *Phd2* knockdown mouse. (**A**) Schematic of *Phd2*-targeted shRNA transgenic strains, *CAG-rtTA;TRE-shPhd2*. These shPhd2 mice express a *CAG*-promoted tetracycline reverse transactivator (*rtTA*). In the presence of doxycycline (Dox) the transcription of an mRNA encoding *GFP* and a silencing shRNA directed against *Phd2* occurs. Control mice express the *CAG-rtTA* but not the shRNA/GFP cassette. (**B**) Representative GFP and brightfield images of shPhd2#9-KH2 ES cells (*R26-rtTA+/-;TRE-Phd2#9+/-*) after 2 days of doxycycline (1.0μg/mL in culture medium) treatment. Scale bar: 100μm. Time-course response of mRNA levels of the target gene (*Phd2*) and the downstream transcriptional effect of HIF-accumulation on *Phd3* mRNA in *shPhd2#9*-KH2 ES cells during Dox-ON and OFF treatment (n=3, values

calculated relative to *Actb* (*bActin*) expression). Data are represented as means ± SD. The western blot (WB) shows the respective protein levels. (**C**) Representative GFP and brightfield images of organs harvested after 2 weeks of doxycycline treatment (2mg/mL with 30% sucrose drinking-water *ad libitum*) in shPhd2#9 and littermate control (Ctrl) mice. Peripheral lymph nodes (pLNs) and bone marrow (BM) following 4 weeks of doxycycline treatment. SI; Small Intestine, SKM; Leg Skeletal Muscle. Scale bar: 1cm. (**D**) Tissue distribution of *Phd2*, HIF target genes (*Phd3* and *Bnip3*) and non-HIF target genes (*Actb*) in organs harvested following two weeks of doxycycline treatment of shPhd2#9 mice and their littermate controls (Ctrl) (n=3, values calculated relative to *Hprt* expression as the relative quantity (RQ) compared with the liver from Ctrl mice). Data are represented as means ± SD. (**E**) Western blot data of HIF1α, HIF2α (arrow), PHD2, and loading control ACTB in the liver harvested following two weeks of doxycycline treatment of shPhd2#9 mice and their littermate controls (Ctrl). (**F**) Reversibility of changes to *GFP* and *Phd2* mRNA levels in doxycycline treated shPhd2#9 (Blue) mice and their littermate controls (Ctrl, Pink) in the liver. Dox-ON group (8 weeks of doxycycline treatment, Solid lines). Dox-ON/OFF group (2 weeks of doxycycline treatment followed by 2 weeks without doxycycline treatment, Dotted lines). N=3 at each time point in both groups, values calculated relative to *Hprt* expression. Data are represented as means ± SD.

Supplementary Figure 2. Similar phenotypes develop in mice bearing a different shRNA sequence knocking down *Phd2*, shPhd2#3. (**A**) Tissue weight of peripheral lymph nodes (pLNs) (x4) and spleens from shPhd2#3 (*Phd2* knockdown) (n=2) and littermate control (Ctrl, n=1) mice treated with doxycycline in the drinking water (2mg/mL with 30% sucrose drinking-water *ad libitum*) for 8 weeks. H&E staining of tissues from shPhd2#3 mice: pLNs (x2.5 (**B**), x10 (**C**) and x40 (**D**)), arrows indicate cells with oval, vesicular nuclei and eosinophilic cytoplasm; spleen (x5 (**E**)); kidney (x20 (**F**) and x40 (**G**)); lung (x20 (**H**)); liver (x40 (**I**)); skin (x80 (**J**), arrows demonstrate exocytosis of lymphocytes into the epidermis). The scale bar is 500μm at x2.5 and proportionately smaller lengths at higher magnifications. The same experiment was repeated twice independently.

Supplementary Figure 3. Time course of changes in body weight and blood count differential after *Phd2* knockdown. (**A**) Body weight (**B**) red blood cell (RBC) counts, (**C**) white blood cell (WBC) counts and (**D**) platelet (Plt) counts from shPhd2#9 (*Phd2* knockdown) and littermate control (Ctrl) mouse blood. Mice were treated for 8 weeks with doxycycline (2mg/mL with 30% sucrose drinking-water *ad libitum*). Data are represented as means ± SD, with n=3-8 per group at each time point gathered in two independent experiments. Groups were compared using a two-way ANOVA.

**p*<0.05; *****p*<0.0001; ns=not significant.

Supplementary Figure 4. Gating strategy for FACS analysis. Representative flow cytometry dot plots indicating the gating strategy **(A)** for identification of myeloid and lymphocyte populations in Figures 2, 4, and 5, and **(B)** for $CD4^+$ lymphocyte subsets in Figures 6, 9 and 10. Control flow plots in Figure 6A, 6B, 9A, and 10 are reshown.

Supplementary Figure 5. *Phd2*, *Hif1a*, and *Hif2a* silencing in doxycycline-induced knockdown mice. mRNA levels of *Phd2*, *Hif1a*, *Hif2a* in the (**A**) liver and (**B**) spleen, harvested from shPhd2#9 (*Phd2* knockdown), shPhd2Hif1 (*Phd2* knockdown/*Hif1a* knockdown), shPhd2Hif2 (*Phd2* knockdown/*Hif2a* knockdown) and control (Ctrl) mice treated for 4 weeks with doxycycline (2mg/mL with 30% sucrose drinking-water *ad libitum,* RQ values against tissues from Ctrl mice). Data are represented as means ± SEM with n=3 per group. Multigroup comparisons were analyzed by one-way ANOVA with Tukey's multiple comparisons post hoc test.

**p*<0.05; ***p*<0.01; ****p*<0.001; ns=not significant.

Supplementary Figure 6. Enumeration of cells bearing helper, effector and regulatory markers in *Phd2* knockdown and knockout mice. (**A**) Gating strategy of single positive ($CD4^+CD8^-$ or $CD4^-CD8^+$), double positive ($CD4^+CD8^+$) and double negative ($CD8^-CD4^-$) cells within spleen of control (Ctrl) and shPhd2#9 mice following 4 weeks of doxycycline treatment (2mg/mL with 30% sucrose drinking-water *ad libitum*). Absolute counts of each population per spleen (left) and expressed as a percentage of $CD3^+$ cells are shown. (**B**) Expression of Foxp3 and CD25 within $CD4^+$ populations within spleen of control (Ctrl) and shPhd2#9 mice following 4 weeks

of doxycycline treatment. Representative dot plots and quantitation both as absolute counts per spleen and percentage amongst total $CD4^+$ cells are shown (**C**) $CD3^+CD4^+Foxp3^+$ cell numbers in spleen and bone marrow (femur) from shPhd2#9 (*Phd2* knockdown), shPhd2Hif1 (*Phd2* knockdown/*Hif1a* knockdown), shPhd2Hif2 (*Phd2* knockdown/*Hif2a* knockdown) and Ctrl mice. (**D**) $CD3^+CD4^+Foxp3^+$ cell numbers in spleen and bone marrow (Femur) from Phd2ko (*Phd2* knockout), Phd2Hif1ko (*Phd2* knockout/*Hif1a* knockout), Phd2Hif2ko (*Phd2* knockout/*Hif2a* knockout) and Ctrl mice. Data are represented as means ± SEM with at least n=3 per group. Unpaired, independent groups of 2 were analyzed using a 2-tailed Student's *t* test. Multigroup comparisons were analyzed by one-way ANOVA with Tukey's or Dunnett's multiple comparisons post hoc test.

*p<0.05; **p<0.01; ***p<0.001.

Supplementary Figure 7. Expression patterns of T cell related cytokines and transcription factors in shPhd2#9 mice. (**A**) Representative flow cytometry plots demonstrating expression of T-bet, TNF-α, IFN-γ, IL-4, GATA-3, IL-17, RORγt, IL-2 and IL-10 against Foxp3 within the total $CD4^+$ populations from spleen of control (Ctrl, left) and shPhd2#9 mice (right) following 4 weeks of doxycycline treatment (2mg/ml with 30% sucrose drinking-water *ad libitum*). (**B**) Percentage of cells expressing T-bet, TNF-α, IFN-γ, IL-4, GATA-3, IL-17, RORγt, IL-2 and IL-10 within $CD4^+Foxp3^-$ (left) or $CD4^+FoxP3^+$ cell populations (right) from spleens of Ctrl and shPhd2#9 mice after 4 weeks of doxycycline treatment (n = 6 mice per group). Data are represented as means ± SEM, analyzed using 2-tailed Student's *t* tests.

*p<0.05; **p<0.01; ***p<0.001; ****p<0.0001; ns=not significant

Supplementary Figure 8. Identification of naïve and memory T cells in shPhd2#9 mice. Dot plots and quantification of naïve (T_N, $CD44^{lo}CD62L^{hi}$), central memory (T_{CM}, $CD44^{hi}CD62L^{hi}$) and effector memory (T_{EM}, $CD44^{hi}CD62L^{lo}$) T cells within spleens of control (Ctrl, left) and shPhd2#9 mice (right) following 4 weeks of doxycycline treatment (2mg/ml with 30% sucrose drinking-water *ad libitum*) (n = 6 mice per group). Data are represented as means ± SEM, analyzed using 2-tailed Student's *t*-tests.

**p<0.01; ***p<0.001; ****p<0.0001; ns=not significant.

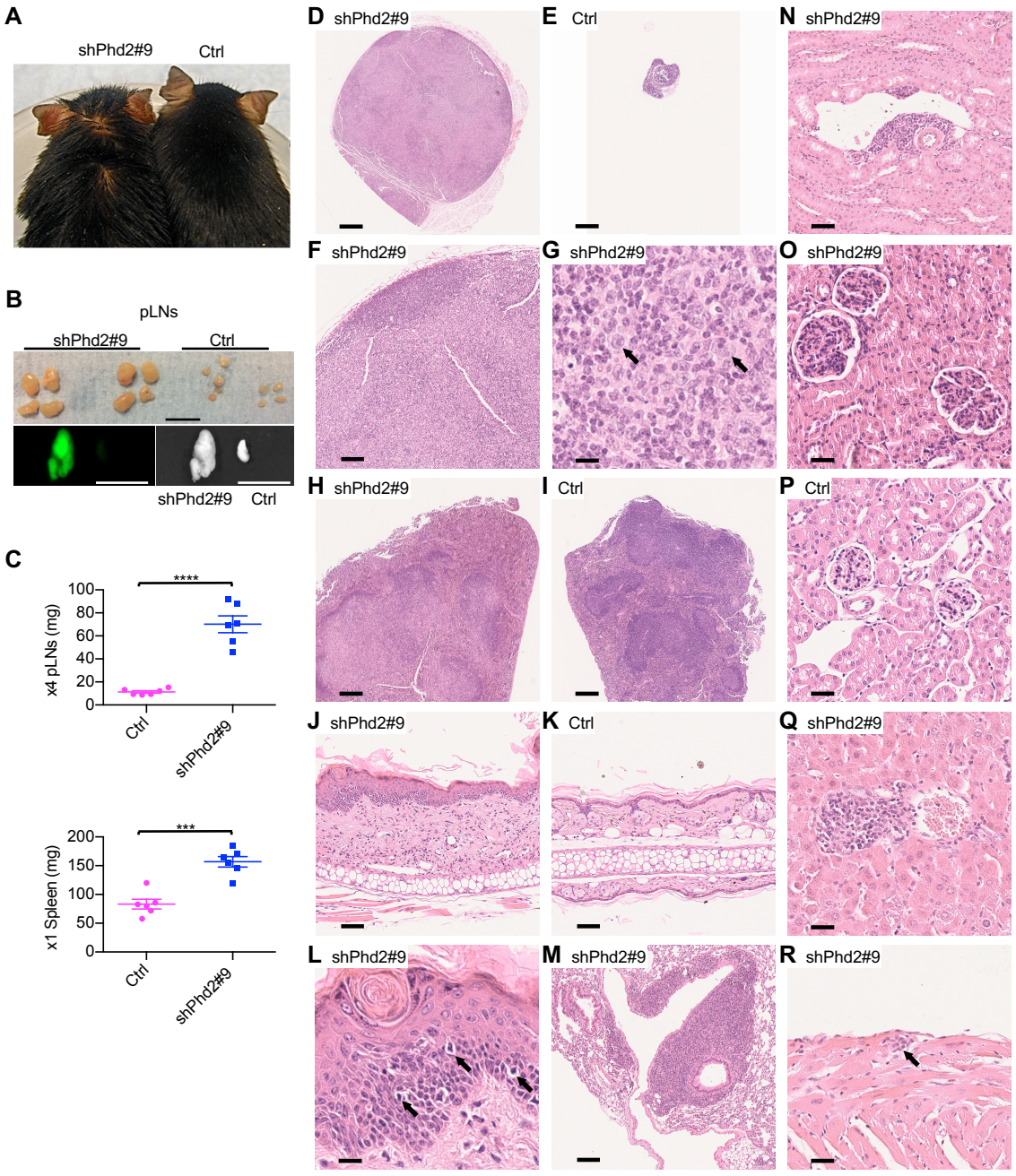

Figure 1. shPhd2#9 mice develop leukocyte expansion on doxycycline treatment. (**A**) Representative image of a shPhd2#9 mouse and its littermate control (Ctrl) treated with doxycycline (2mg/mL with 30% sucrose drinking-water *ad libitum*) for 4-5 weeks. (**B**) Representative brightfield and GFP images of peripheral lymph nodes (pLN) from a shPhd2#9 mouse and its littermate control (Ctrl). Scale bar: 1cm (**C**) Wet weight of pLNs (x4) and spleens (x1) from shPhd2#9 mice (n=6) and their littermate control (Ctrl, n=6). Unpaired, independent groups of 2 were analyzed using a 2-tailed Student's *t* test. Data are represented as means ± SEM. H&E staining of tissues from shPhd2#9 and littermate control (Ctrl) mice: pLN (x2.5 (**D**-**E**), x10 (**F**) and x80 (**G**)), arrows indicate cells with oval, vesicular nuclei and eosinophilic cytoplasm; spleen (x5 (**H**-**I**)); skin (x20 (**J**-**K**) and x80 (**L**)), arrows demonstrate exocytosis of lymphocytes into the epidermis; lung (x10 (**M**)); kidney (x20 (**N**) and x40 (**O**-**P**)); liver (x40 (**Q**)); heart (x40 (**R**)), arrow indicates a focal collection of mononuclear inflammatory cells at the epicardial surface of the heart. The scale bar is 500µm at x2.5 and proportionately smaller lengths at higher magnifications. Each symbol in (**C**) represents an individual mouse. Data are representative of those obtained in three independent experiments at this time point.

***p<0.001; ****p<0.0001.

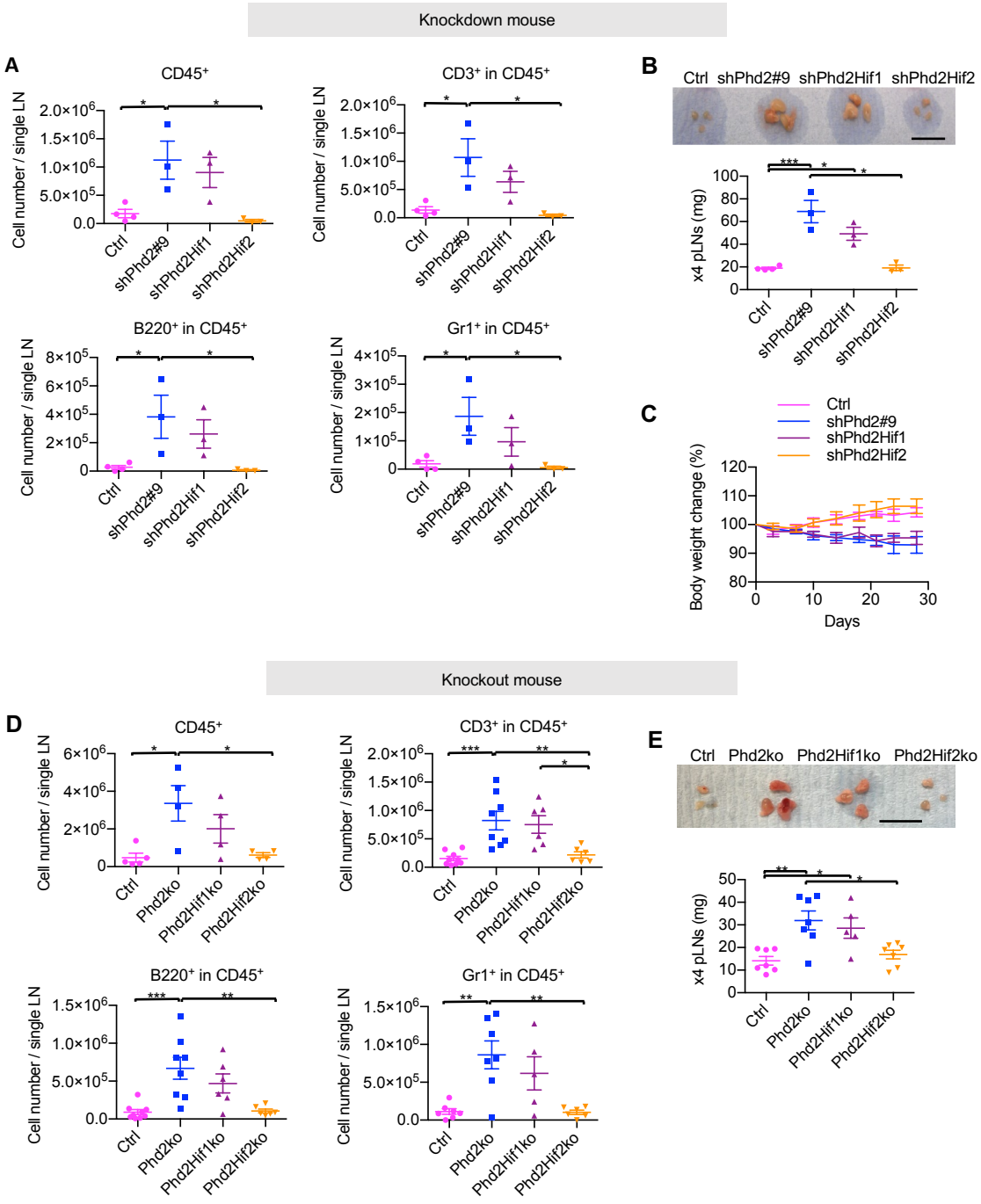

Figure 2. Reduction of *Hif2a* expression reverses the phenotype in inducible *Phd2* knockdown and *Phd2* knockout mice. (**A**) FACS analysis of cells in peripheral lymph nodes (pLNs) from shPhd2#9 (*Phd2* knockdown), shPhd2Hif1 (*Phd2* knockdown/*Hif1a* knockdown), shPhd2Hif2 (*Phd2* knockdown/*Hif2a* knockdown) and control (Ctrl) mice for CD45, CD3, B220, and Gr1 expression. Mice were treated with doxycycline (2mg/mL with 30% sucrose drinking-water *ad libitum*) for 4 weeks. Data from individual mice and means ± SEM are represented. Groups were compared using a one-way ANOVA with Tukey's post hoc tests. (**B**) Representative brightfield images and wet weight of peripheral lymph nodes (pLN) from the same mice. Data are represented as means ± SEM. Scale bar: 1cm. (**C**) Mean body weight changes (% relative to day 0) of the same mice during doxycycline treatment. Data are represented as means ± SD, with at least n=3 per group. Groups were compared by a repeated measures ANOVA with Tukey's multiple comparisons post hoc test: Ctrl vs shPhd2#9 (***); Ctrl vs shPhd2Hif1 (**); Ctrl vs shPhd2Hif2 (ns); shPhd2#9 vs shPhd2Hif1 (ns); shPhd2#9 vs shPhd2Hif2 (***); shPhd2Hif2 vs shPhd2Hif1 (***). (**D**) FACS analysis for CD45, CD3, B220, and Gr1 expression by cells in pLNs from conditional Phd2ko (*Phd2* knockout), Phd2Hif1ko (*Phd2* knockout/*Hif1a* knockout), Phd2Hif2ko (*Phd2* knockout/*Hif2a* knockout) and control (Ctrl) mice 4 weeks after tamoxifen treatment. Data from individual mice and means ± SEM are represented. Groups were compared using a one-way ANOVA with Tukey's post hoc tests. (**E**) Representative brightfield images and wet weight of pLNs from the same mice. Data are represented as means ± SEM. Scale bar: 1cm. Multigroup comparisons were analyzed by a one-way ANOVA with Tukey's multiple comparisons post hoc test. Each symbol in (**A**)-(**E**) represents an individual mouse. Data were consistent over three independent experiments.

*p<0.05; **p<0.01; ***p<0.001; ns=not significant.

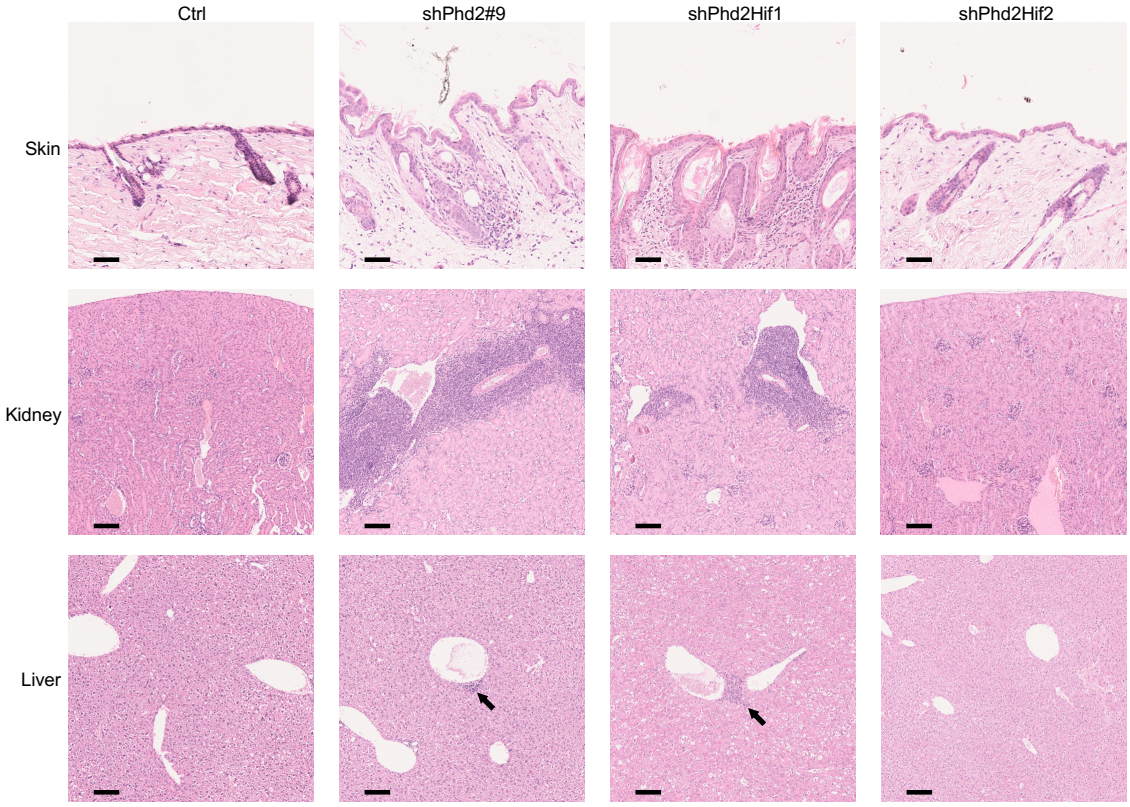

Figure 3. Concomitant *Hif2a* silencing ablates tissue inflammation in *Phd2* knockdown mice. H&E staining of skin (x20), kidney (x10) and liver (x10, arrows demonstrate periportal and perivenous mononuclear inflammatory cell infiltrates) from shPhd2#9 (*Phd2* knockdown), shPhd2Hif1 (*Phd2* knockdown/*Hif1a* knockdown), shPhd2Hif2 (*Phd2* knockdown/*Hif2a* knockdown) and control (Ctrl) mice treated for 4 weeks with doxycycline. The scale bar is 125μm at x10 and proportionately smaller lengths at higher magnifications. Each column of images is representative of multiple sections from each organ from the same mouse. In this experiment tissues form two mice of each genotype were examined.

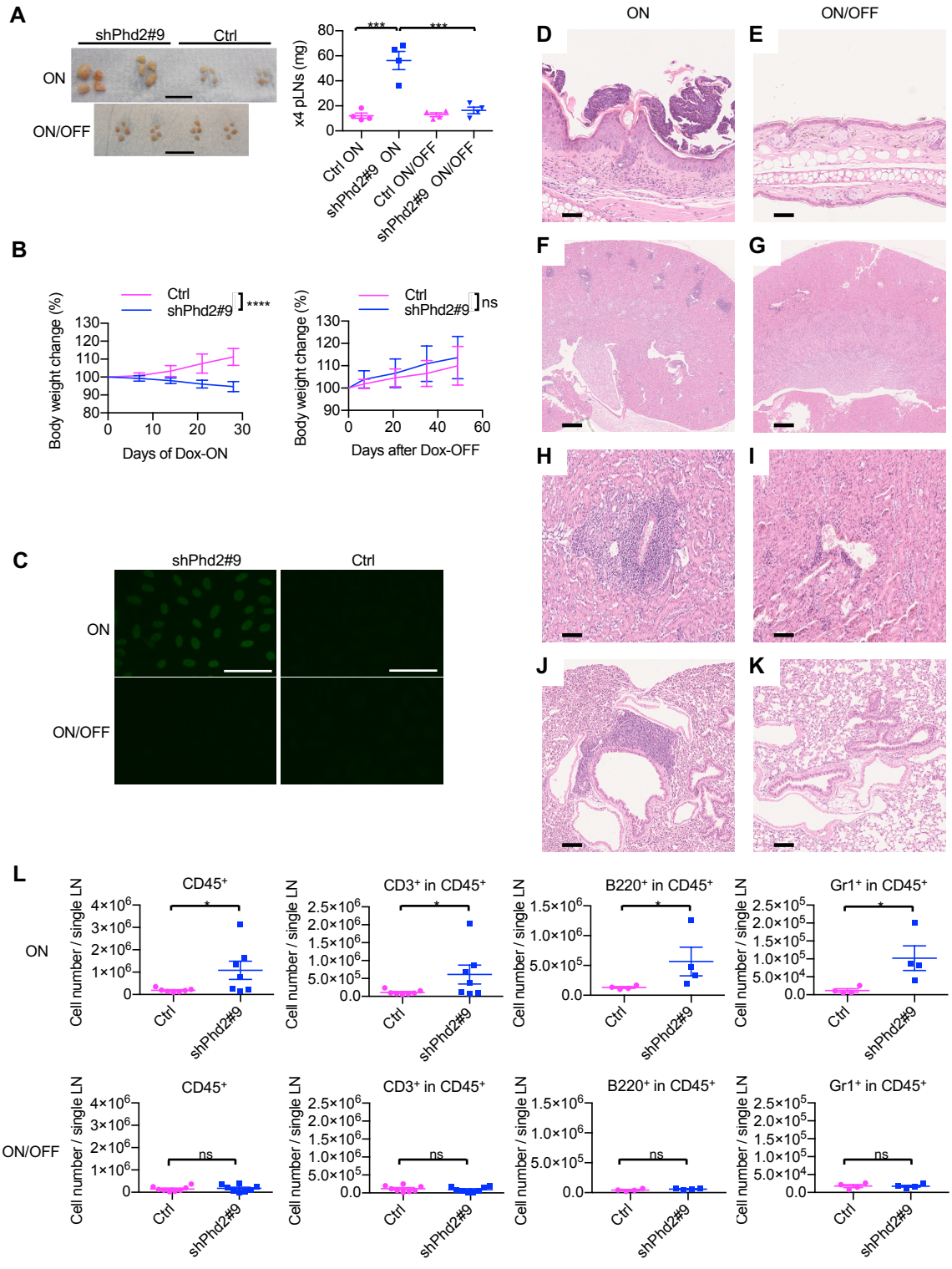

Figure 4. Phenotype reversal following withdrawal of doxycycline. (**A**) Representative brightfield images and wet weight of peripheral lymph nodes (pLNs) from shPhd2#9 mice and their littermate controls (Ctrl) maintained on doxycycline for 3-4 weeks (Dox-ON group) or treated with doxycycline for 3-4 weeks and then analyzed 7 weeks after doxycycline withdrawal (Dox-ON/OFF group). Scale bars: 1cm. Data are represented as means ± SEM with n=4 per group. Multi-group comparisons were analyzed by one-way ANOVA with Tukey's multiple comparisons post hoc test. (**B**) Mean body weight changes (%) of shPhd2#9 and Ctrl mice, relative to day 0 of doxycycline treatment or doxycycline withdrawal. Data are represented as means ± SD, with n=7-8 per group. Groups were compared using a two-way ANOVA. (**C**) Representative fluorescent image of anti-nuclear antibodies (ANA) using mouse serum from Dox-ON and Dox-ON/OFF groups of shPhd2#9 and Ctrl mice. Scale bars: 50μm. H&E staining of skin (x20 (**D**-**E**)), kidney (x2.5 (**F**-**G**); x10 (**H**-**I**)) and lung (x10 (**J**-**K**)) from Dox-ON and Dox-ON/OFF groups of shPhd2#9 mice. The scale bar is 500 μm at x2.5 and proportionately smaller lengths at higher magnifications. (**L**) FACS analysis of cells from pLNs from Dox-ON and Dox-ON/OFF groups of shPhd2#9 and Ctrl mice, analyzed for CD45, CD3, B220 and Gr1 expression. Data are represented as means ± SEM with at least n=4 per group. Unpaired, independent groups of 2 were analyzed using a 2-tailed Student's *t* test. Each symbol in (**A**) and (**L**) represents an individual mouse. Data were consistent over two independent experiments.

*p<0.05; ***p<0.001; ****p<0.0001; ns=not significant.

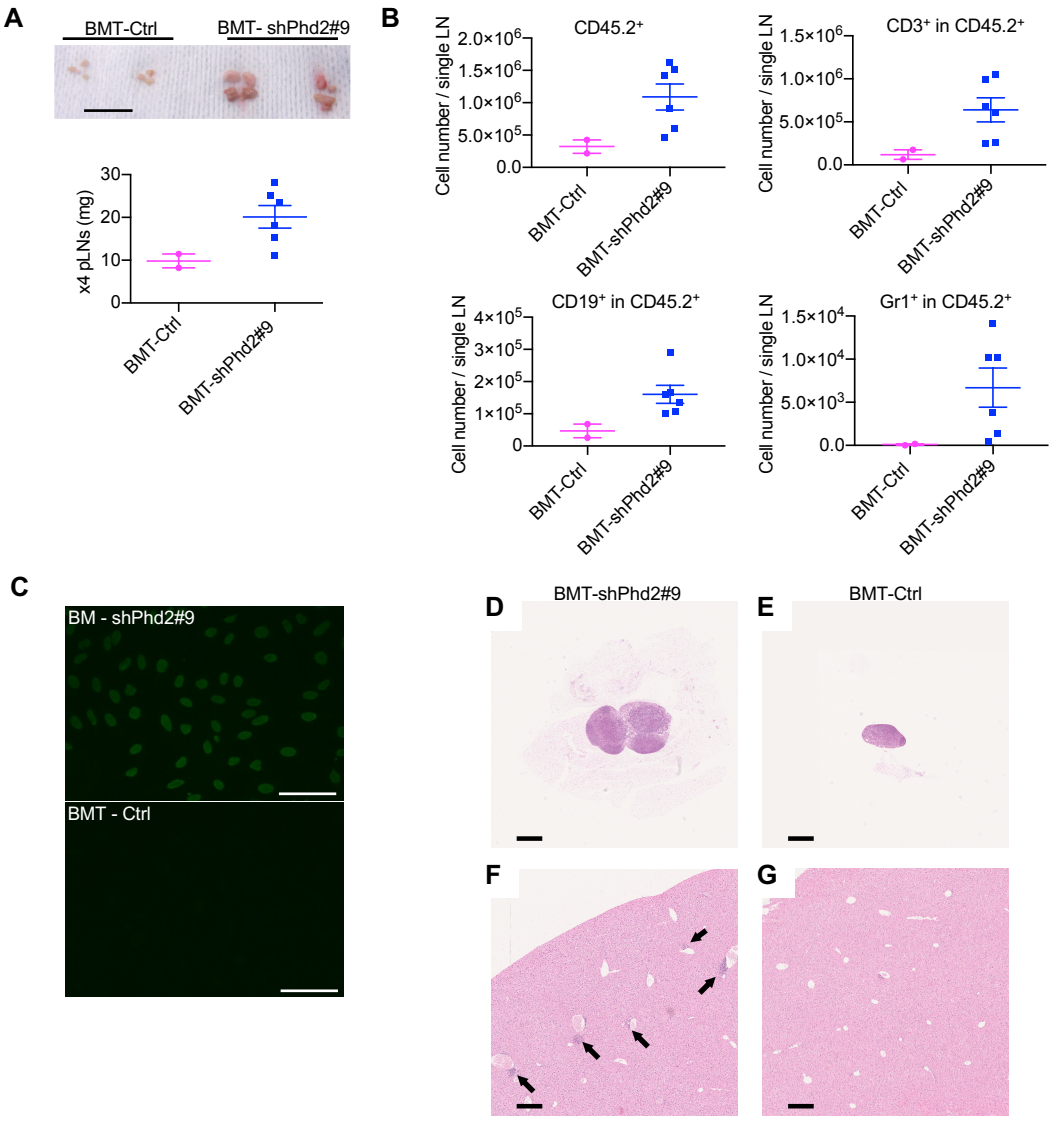

Figure 5. Transfer of the *Phd2* knockdown phenotype by bone marrow transplantation (BMT). (**A**) Representative brightfield images and tissue weights of peripheral lymph nodes (pLN) from BMT recipients following 10 weeks treatment with doxycycline (2mg/mL with 30% sucrose drinking-water *ad libitum*). Syngeneic congenically marked (CD45.1) mice were lethally-irradiated before receiving CD45.2 shPhd2#9 bone marrow (BMT-shPhd2#9, n=6) or CD45.2 control bone marrow (BMT-Ctrl, n=2) and allowed to reconstitute for 8 weeks prior to doxycycline treatment. Scale bars: 1cm. Data are represented as means ± SEM. (**B**) FACS analysis of cells in pLNs from BMT-Ctrl and BMT-shPhd2#9 mice, analyzed for $CD45.2^+$, $CD45.2^+CD3^+$, $CD45.2^+CD19^+$, and $CD45.2^+Gr1^+$ expression. Data are represented as means ± SEM. (**C**) Representative fluorescent image of anti-nuclear antibodies (ANAs) using mouse serum from BMT recipients. Scale bars: 50μm. H&E staining of the pLN (x2.5 (**D**-**E**)) and liver (x5 (**F**-**G**)) from BMT recipient mice. Arrows indicate inflammatory foci. The scale bar is 500μm at x2.5 and proportionately smaller lengths at higher magnifications. Each symbol in (**A**) and (**B**) represents an individual mouse. The same experiment was repeated twice independently.

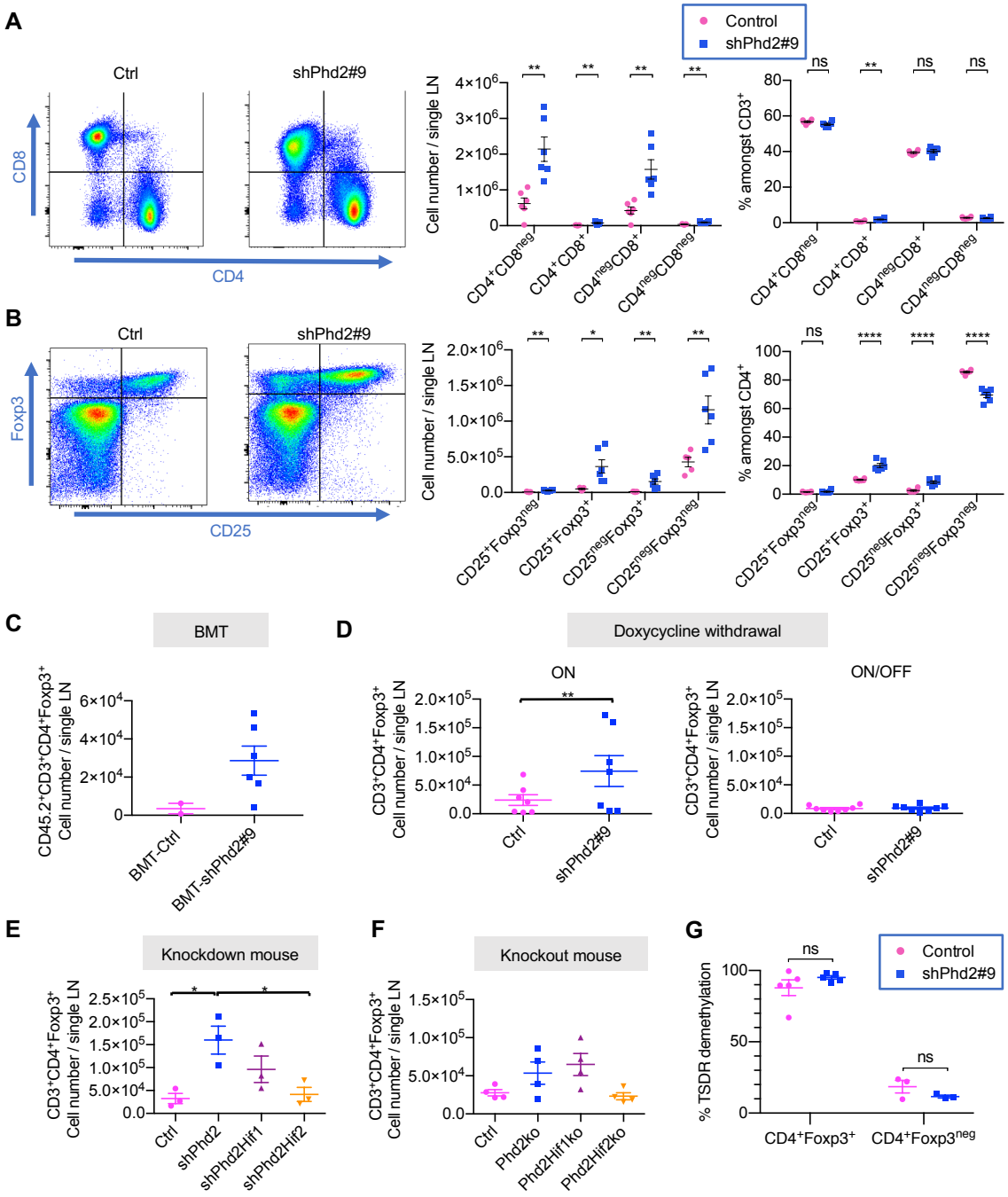

Figure 6. Enumeration and TSDR analysis of cells bearing helper, effector and regulatory markers in *Phd2* knockdown and knockout mice. (**A**) Gating strategy and enumeration of single positive ($CD4^+CD8^-$ or $CD4^-CD8^+$), double positive ($CD4^+CD8^+$) and double negative ($CD8^-CD4^-$) cells within lymph nodes (pLNs) of control (Ctrl) and shPhd2#9 mice following 4 weeks of doxycycline treatment (2mg/mL with 30% sucrose drinking-water *ad libitum*). (**B**) Expression of Foxp3 and CD25 within $CD4^+$ populations within lymph nodes (pLNs) of control (Ctrl) and shPhd2#9 mice following 4 weeks of doxycycline treatment. (**C**) $CD45.2^+CD3^+CD4^+Foxp3^+$ cell numbers in pLNs from lethally-irradiated syngeneic $CD45.1^+$ congenically marked mice receiving bone marrow transplants (BMT) from $CD45.2^+$ shPhd2#9 or $CD45.2^+$ Ctrl mice. (**D**) $CD3^+CD4^+Foxp3^+$ cell numbers in the peripheral lymph nodes (pLNs) of shPhd2#9 mice and their littermate controls (Ctrl), treated with doxycycline for 3-4 weeks and analyzed directly (ON) or 7 weeks after doxycycline withdrawal (ON/OFF) (n=7-8, two independent assays). (**E**) $CD3^+CD4^+Foxp3^+$ cell numbers in pLNs from shPhd2#9 (*Phd2* knockdown), shPhd2Hif1 (*Phd2* knockdown/*Hif1a* knockdown), shPhd2Hif2 (*Phd2* knockdown/*Hif2a* knockdown) and Ctrl mice. (**F**) $CD3^+CD4^+Foxp3^+$ cell numbers in pLNs from Phd2ko (*Phd2* knockout), Phd2Hif1ko (*Phd2* knockout/*Hif1a* knockout), Phd2Hif2ko (*Phd2* knockout/*Hif2a* knockout)and Ctrl mice. (**G**) Flow sorted $CD4^+Foxp3^+$ or $CD4^+Foxp3^-$ cells from Ctrl or shPhd2#9 mice that were treated for 4 weeks with doxycycline were analyzed for the percentage demethylation of their TSDR on the active X chromosome by pyrosequencing. Data are represented as means ± SEM with at least n=3 per group. Unpaired, independent groups of 2 were analyzed using a 2-tailed Student's *t* test. Multigroup comparisons were analyzed by one-way ANOVA with Tukey's or Dunnett's multiple comparisons post hoc test. TSDR data were analyzed by two-way ANOVA with Šídák's correction for multiple comparisons. Each symbol represents an individual mouse. Data in panels (**C**)-(**G**) are representative of two independent experiments.

**p*<0.05; ***p*<0.01; ****p*<0.001.

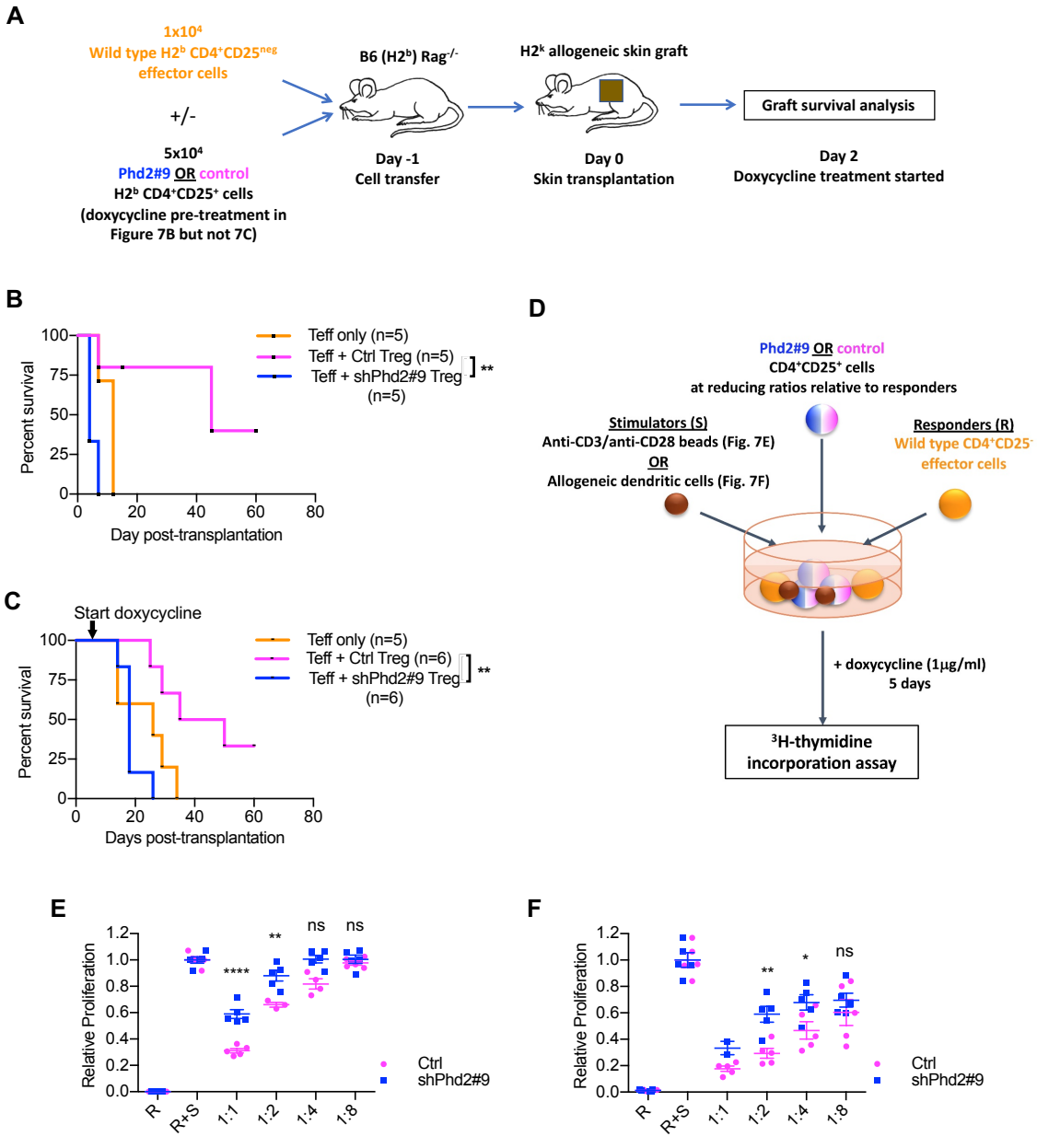

Figure 7. Treg functional assays. (**A**) Schematic of *in vivo* experimental plan. C57BL/6 Rag1$^{-/-}$ (H-2^{b}) mice received CD4^{+}CD25^{-} effector T cells (Teff) with or without H2^{b} CD4^{+}CD25^{+} cells from shPhd2#9 or control (Ctrl) mice that had either received 1 week doxycycline (2mg/ml in drinking water, *ad libitum*) pre-treatment or no doxycycline pre-treatment. One day later, mice received an allogeneic H-2^{k} skin graft. Mice receiving cells from doxycycline treated donors remained on doxycycline (**B**) whereas those receiving cells from untreated donors started doxycycline treatment from day 2 after transplantation (**C**). Allograft survival was monitored until rejection. (**B**) Survival graph with adoptively transferred cells derived from 1 week doxycycline pre-treated mice. (**C**) Survival graph with adoptively-transferred cells derived from mice only treated with doxycycline after adoptive transfer. Survival data were analyzed using the log-rank test for both **(B)** and **(C)**. The number of animals in each group is indicated. **(D)** Schematic of *in vitro* experimental plan. 1x10^{5}/well control C57BL/6 WT Teffs (CD4^{+}CD25^{-} responders, R) were stimulated (S) with 1x10^{5}/well anti-CD3/anti-CD28 beads or 2x10^{4} CBA (H-2^{k}) dendritic cells (DCs). CD4^{+}CD25^{+} cells from shPhd2#9 or Ctrl mice were added at 1:1, 1:2, 1:4 and 1:8 ratios relative to Teff responders. Doxycycline at 1μg/mL was added to all wells and replenished daily. Cells were incubated for 5 days and ^{3}H-thymidine added for the final 18 hours of culture. Proliferation levels were normalized to positive control (R+S). (**E**) *In vitro* suppression assay using anti-CD3/anti-CD28 as stimulators. (**F**) *In vitro* suppression assay using DCs as stimulators. Data are represented as means ± SEM of biological replicates. Unpaired, independent groups (1:1, 1:2, 1:4, and 1:8) of 2 were analyzed using 2-tailed Student's *t* tests in (**E**) and (**F**).

*p<0.05; **p<0.01; ****p<0.0001; ns=not significant.

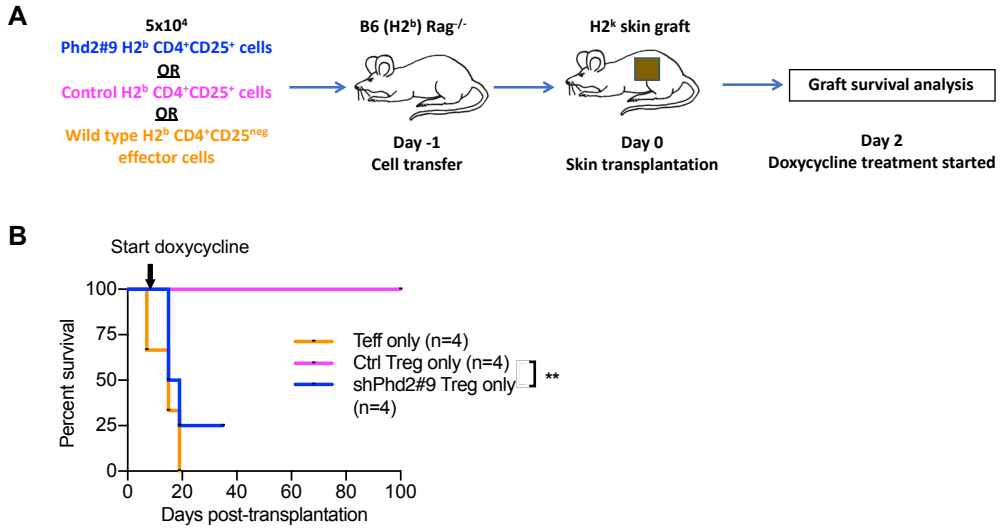

Figure 8. *Phd2* knockdown CD4⁺CD25⁺ cells alone can induce skin allograft rejection. (**A**) Schematic of *in vivo* experimental plan. C57BL/6 Rag1$^{-/-}$ (H-2^{b}) mice received either: 5x10^{4} H2^{b} CD4^{+}CD25^{+} cells from shPhd2#9 mice; 5x10^{4} H2^{b} CD4^{+}CD25^{+} cells from control (Ctrl) mice; or 5x10^{4} H2^{b} wild type CD4^{+}CD25^{-} effector cells alone. One day later, mice received an allogeneic H-2^{k} skin graft, followed by doxycycline treatment (2mg/ml in drinking water, *ad libitum*) from day 2 post-transplantation. Allograft survival was monitored until rejection. The number of animals in each group is indicated. (**B**) Skin allograft survival graph. Survival data were analyzed using the log-rank test. The censored datapoint in the shPhd2#9 group represents a mouse that developed weight loss and a generalized inflammatory phenotype.

**p<0.01

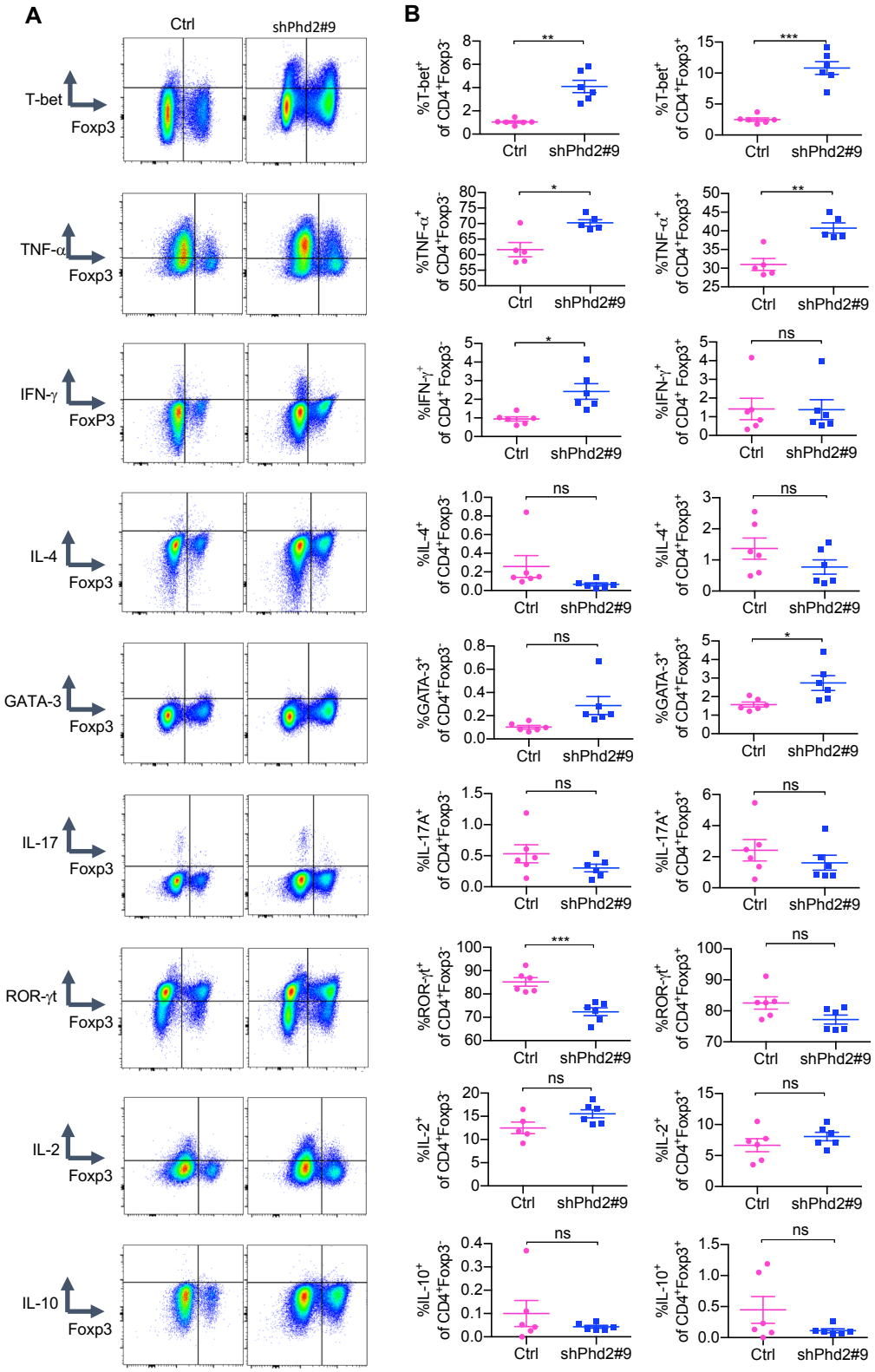

Figure 9. Expression patterns of T cell related cytokines and transcription factors in shPhd2#9 mice. (**A**) Representative flow cytometry plots demonstrating expression of T-bet, TNF-α, IFN-γ, IL-4, GATA-3, IL-17, ROR-γt, IL-2 and IL-10 against Foxp3 within the total CD4⁺ populations from lymph nodes (pLNs) of control (Ctrl, left) and shPhd2#9 mice (right) following 4 weeks of doxycycline treatment (2mg/ml with 30% sucrose drinking-water *ad libitum*). (**B**) Percentage of cells expressing T-bet, TNF-α, IFN-γ, IL-4, GATA-3, IL-17, ROR-γt, IL-2 and IL-10 within CD4⁺ Foxp3⁻ (left) or CD4⁺ FoxP3⁺ cell populations (right) from pLNs of Ctrl and shPhd2#9 mice after 4 weeks of doxycycline treatment (n = 6 mice per group). Data are represented as means ± SEM, analyzed using 2-tailed Student's *t* tests.

*p<0.05; **p<0.01; ***p<0.001; ****p<0.0001; ns=not significant

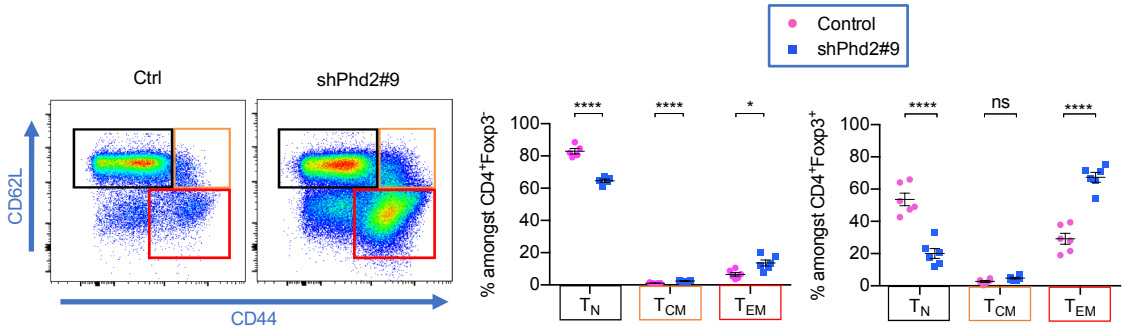

Figure 10. Identification of naïve and memory T cells in shPhd2#9 mice. Dot plots and quantification of naïve (T_N, $CD44^{lo}CD62L^{hi}$), central memory (T_{CM}, $CD44^{hi}CD62L^{hi}$) and effector memory (T_{EM}, $CD44^{hi}CD62L^{lo}$) T cells within pLNs of control (Ctrl, left) and shPhd2#9 mice (right) following 4 weeks of doxycycline treatment (2mg/ml with 30% sucrose drinking-water *ad libitum*) (n = 6 mice per group). Data are represented as means ± SEM, analyzed using 2-tailed Student's *t*-tests.

***p*<0.01; ****p*<0.001; *****p*<0.0001; ns=not significant.